

Experimental Investigation of Water Droplet Impact and Icing on Hydrophobic Surfaces with Varying Wettabilities

by Yuntao Pan

A thesis submitted to the School of Graduate Studies
in partial fulfilment of the requirements for the degree of

Master of Engineering

Faculty of Engineering and Applied Science
Memorial University of Newfoundland

May 2018

St. John's, Newfoundland, Canada

Abstract

Ice formation and accumulation can lead to operational failure and risks for structures such as power transmission lines, aircrafts, offshore platforms, marine vessels, and wind turbines. Liquid repellent surfaces could reduce ice accretion and improve asset integrity and safety in harsh environments. There are significant needs to probe how surface wettability affects the droplet impact, ice formation and ice accretion processes. This study presents experimental results of water droplet impact, droplet dynamics, and icing delay time on flat and inclined stainless-steel surfaces with varying wettabilities. Several different designs of the micro-structure of the hydrophobic surfaces are considered. The commercial hydrophobic coating from Aculon is also used to improve liquid repellency and reduce ice accumulation. It was found that the impact speed and surface wettability are significant factors to the droplet oscillation and the total icing time. The droplet oscillation time is significantly longer on a hydrophobic surface than on a hydrophilic one. Lower surface wettability also significantly increases the droplet total icing time. The droplet total icing time decreases with lower droplet temperature, larger droplet impact velocity, and smaller droplet diameter. The droplet shows a gliding phase on an inclined surface. The total icing time decreases on the inclined surface since the contact area increases due to the gliding process. For typical droplet icing process, the ice formation initiates at the solid-liquid interface and then propagates from bottom to top through the liquid-gas interface. The droplet bounces off from the angled superhydrophobic surface made by electrodeposition at room temperature.

Acknowledgements

It is a great pleasure to acknowledge my deepest thanks and gratitude to **Dr. Xili Duan**, Assistant Professor, Faculty of Engineering and Applied Science at the Memorial University of Newfoundland, for suggesting the topic of this thesis, and his kind supervision. It is a great honour to work under his supervision.

I would like to express my deepest thanks and sincere appreciation to **Dr. Greg Naterer**, Dean of the Faculty of Engineering and Applied Science at the Memorial University of Newfoundland, for his mentor, creative and comprehensive advice to make this work comes true.

I sincerely appreciate the financial support from Petroleum Research Newfoundland & Labrador (PRNL) and the Natural Sciences and Engineering Research Council of Canada (NSERC) to make this research happen.

I sincerely appreciate my parents for their great help and encourage in my life.

Many thanks and appreciations also go to my colleague and all the people who have kindly helped me with their knowledge during my research time.

List of Abbreviations and Symbols

d_m	Maximum spreading diameter [m]
D	Initial droplet diameter [m]
f	Solid-liquid surface contact area fraction
$f(\eta, x)$	Geometrical factor
m	Droplet mass [kg]
Oh	Ohnesorge number
r	Roughness ratio of actual area to apparent area
r_f	Roughness ratio of the wet surface area in Cassie-Baxter Model
Re	Reynold number
t_c	Total time the droplet in contact with substrate [s]
t^*	Dimensionless time scale
T_s	Temperature of solid surface [°C]
u	Droplet impact velocity [m/s]
WEDM	Wire Electrical Discharge Machining
We	Weber number
α	Thermal diffusivity [m^2/s]
a_{ns}	Thermal diffusivities of the solid-air domain [m^2/s]
a_w	Thermal diffusivities water domain [m^2/s]
γ_{sv}	Solid-vapor interfacial tension [N/m]
γ_{lv}	Liquid-vapor interfacial tension [N/m]
γ_{sl}	Solid-liquid interfacial tension [N/m]
θ	Static contact angle [°]
θ_a	Advancing contact angle [°]

θ_{CB}	Static contact angle under Cassie-Baxter state [°]
θ_s	Static contact angle on a smooth surface of the same material [°]
θ_W	Static contact angle under Wenzel state [°]
μ	Viscosity [$Pa \cdot s$]
ξ	Maximum spread factor
ρ	Density [kg/m^3]
σ_{12}	Surface free energy of the interface between 1 and 2 [J]
ΔG^*	Critical free energy barrier
ΔG_v	Free energy difference for unit volume of two different phases [J/m^3]

Table of Contents

Abstract.....	I
Acknowledgements	II
List of Abbreviations and Symbols	III
List of Tables	VII
List of Figures.....	VIII
Chapter 1 Introduction.....	1
1.1 Background.....	1
1.2 Objectives	2
Chapter 2 Literature Review	4
2.0 Introduction.....	4
2.1 Surface Wettability	4
2.2 Metallic Hydrophobic Surface Fabrication.....	7
2.3 Droplet Dynamic on Hydrophobic Surface	9
2.4 Ice Formation on Hydrophobic Surface.....	12
2.5 Experimental Methods	14
2.5.1 Droplet Dynamics	14
2.5.2 Droplet Icing Process.....	16
2.6 Summary	18
Chapter 3 Methodology	19
3.0 Introduction.....	19
3.1 Design of Experiment Technique	19
3.2 Determining the Factors and Levels	21
3.3 Dimensional Analysis	23
3.4 Measurement of the Factors and Responses	24
3.5 Experimental Apparatus	25
3.6 Sample Preparation	28
3.7 Experimental Procedure.....	31
3.8 Summary	33
Chapter 4 Results and Analysis	34
4.0 Introduction.....	34
4.1 Droplet Oscillation time.....	34

4.2 Droplet Impact and Ice Formation Process on the Flat Surface	43
4.3 Droplet Impact and Ice Formation Process on the Inclined Surface	58
4.4 Summary	71
Chapter 5 Conclusion and Recommendation on Future Work	72
4.1 Conclusion	72
4.2 Future Work	74
Reference	75
Appendix I	83

List of Tables

Table 1: Different surface types with their water repellency and mobility.	6
Table 2: Summary of design factors and levels	21
Table 3: Description of various parameters of heat transfer [63]	23
Table 4: The uncertainty table of the equipment used in the experiment	27
Table 5: Static contact angle of different sample surfaces	29
Table 6: Advancing and receding contact angles of different sample surfaces.....	29
Table 7: Detailed run sheet and experimental results	31
Table 8: ANOVA results.....	35
Table 9: The wettability measurement after icing experiment.....	71

List of Figures

Figure 1: A droplet on a smooth or rough surface [20]	6
Figure 2: Advancing and receding angles of a droplet on the tilted surface [20]	7
Figure 3: 1-D transient heat conduction model.....	14
Figure 4: The various droplet impact conditions [27].....	15
Figure 5: The freezing process of a static droplet on the superhydrophobic surface [57]	18
Figure 6: Liquid droplet impact and icing apparatus	27
Figure 7: Experimental systems of droplet impact and icing	28
Figure 8: Schematic diagram of WEDM process [21].....	30
Figure 9: Detail drawings of Channel 1, Channel 2 and varied channel	30
Figure 10: Droplet (with impact speed = 0.77 m/s) oscillation on the surface of the hydrophilic sample. Surface and droplet temperatures are at room temperature of 18.5 °C.	36
Figure 11: Normal plot of residuals	37
Figure 12: Residuals vs. predicted	38
Figure 13: Residuals vs. run.....	38
Figure 14: Predicted result vs. actual experimental result	39
Figure 15: Box-Cox plot for power transformations	39
Figure 16: The interaction plot between droplet temperature and surface wettability. The graph is plotted under surface temperature = -10 °C and impact speed = 0.81 m/s.	40
Figure 17: The interaction plot between surface temperature and surface wettability. The graph is plotted under droplet temperature = 10 °C and impact speed = 0.81 m/s.	41

Figure 18: The interaction plot between impact speed and surface wettability. The graph is plotted under surface temperature = -10 °C and droplet temperature = 10 °C.42

Figure 19: The droplet impact on the 17-4 PH stainless steel sample under different impact speeds. Surface and droplet temperatures are at a room temperature of 18.5 °C, and the diameter of the droplet is 1.80 mm.42

Figure 20: Droplet geometry and imaging scale.....43

Figure 21: Droplet oscillations on the hydrophilic stainless-steel surface, with droplet initial temperature 18.5 °C, impact speed 1 m/s, steel surface temperature -7 °C.43

Figure 22: A Coordinate system of droplet impact movement45

Figure 23: Images of water droplet impact on flat smooth surface ($D=2.82$ mm, $T_s=-10^\circ\text{C}$, $u=0.77$ m/s, $T_d=5^\circ\text{C}$ and $\theta=77^\circ$)46

Figure 24: Images of water droplet impact on flat coated varied channel surface ($D=2.82$ mm, $T_s=-10^\circ\text{C}$, $u=0.77$ m/s, $T_d=5^\circ\text{C}$ and $\theta =145^\circ$).....48

Figure 25: Droplet diameter at liquid-solid interface vs. time ($D=2.82$ mm, $u=0.77$ m/s, and $\theta= -10^\circ\text{C}$)49

Figure 26: Droplet diameter at liquid-solid interface vs. time on smooth surface ($u=0.77$ m/s, and $T_s= -10^\circ\text{C}$).....51

Figure 27: The change of droplet diameter with time on smooth surface ($u= 0.77$ m/s, and $T_s= -10^\circ\text{C}$).....51

Figure 28: Droplet icing time vs. static contact angle at $u= 0.77$ m/s when $T_s= -10^\circ\text{C}$ and -13°C52

Figure 29: Droplet icing time vs. Static contact angle at -10°C when the impact speed is 0.77 m/s, 0.99 m/s, and 1.17 m/s.....53

Figure 30: Droplet icing time vs. Static contact angle at -10°C when the droplet

diameter is 1.8 mm, 2.82 mm, and 4.11 mm.....	54
Figure 31: Dimensionless time vs. impact We at different impact velocities at -10°C	55
Figure 32: Dimensionless time vs. Impact We when the surface temperature is -10 °C and -13 °C.....	56
Figure 33: Dimensionless time vs. f number at different impact velocities	56
Figure 34: The detailed water droplet icing process	57
Figure 35: Water droplet impact and icing comparison on Smooth and coated varied channel surface ($D=2.82$ mm, $T_s=-10^\circ\text{C}$, $u=0.77$ m/s and $T_d=5^\circ\text{C}$)	58
Figure 36: Coordinate system of droplet impact movement on inclined surface	60
Figure 37: Images of water droplet impact on the smooth surface with the inclined angle of 30° ($D=2.82$ mm, $T_s=-10^\circ\text{C}$, $u=0.77$ m/s, $T_d=5^\circ\text{C}$ and $\theta=77^\circ$).....	61
Figure 38: Images of water droplet impact on coated varied channel surface with an inclined angle of 30° ($D=2.82$ mm, $T_s=-10^\circ\text{C}$, $u=0.77$ m/s, $T_d=5^\circ\text{C}$ and $\theta=145^\circ$)....	63
Figure 39: Total icing time vs. Static contact angle at three different inclined angles which are flat, 30° , and 60° . ($D=2.82$ mm, $T_s=-10^\circ\text{C}$, $u=0.77$ m/s, and $T_d=5^\circ\text{C}$).....	63
Figure 40: Images of water droplet impact on the smooth surface with an inclined angle of 60° ($D=2.82$ mm, $T_s=-10^\circ\text{C}$, $u=0.77$ m/s, $T_d=5^\circ\text{C}$ and $\theta=77^\circ$).....	65
Figure 41: Images of water droplet impact on coated varied channel surface with inclined angle of 60° ($D=2.82$ mm, $T_s=-10^\circ\text{C}$, $u=0.77$ m/s, $T_d=5^\circ\text{C}$ and $\theta=145^\circ$)....	67
Figure 42: Images of water droplet impact on electrodeposition with an inclined angle of 60° ($D=2.82$ mm, T_s = room temperature, $u=0.77$ m/s, $T_d=5^\circ\text{C}$, and $\theta=145^\circ$).....	69
Figure 43: The effect of advancing contact angle of sample surface on droplet total icing time with inclined angles of 30° and 60°	70

Chapter 1

Introduction

1.1 Background

In arctic and harsh environments, the formation and accumulation of ice may cause significant hazards to many engineering structures such as power transmission lines, airplanes, wellhead platforms, and marine vessels [1-4]. There are many different inefficient ways to remove ice from structures. For example, a high-frequency high-voltage short-circuit is used to melt the ice, but it requires to shut off power during de-icing operation [5-7]. Workers still need to use hammers to remove the ice on wellhead platforms and chain bridge. These methods are inefficient and suboptimal. Furthermore, they may be expensive, and often have safety and environmental issues [8]. Many commercial coatings can reduce ice formation or ice adhesion, but these commercial coatings may have negative impacts on the environment. Also, the durability is a big issue as the coating depletes during icing and de-icing process [9-11]. In order to find a more efficient and appealing approach to reduce ice formation and adhesion, extensive research has been directed to develop hydrophobic surfaces with water-repellent and anti-icing properties for applications in the harsh environment [8] [12-13]. Surface wettability is a key factor to mitigate wetting and icing on metallic surfaces in the harsh environment.

1.2 Objectives

Since there is no sufficient research on how surface wettability affects the droplet icing time, we aim to find out such a relationship in this study. This study also considers the droplet dynamics and icing process together to analyze the droplet total icing time, which most researchers didn't consider. The correlation between surface wettability and the droplet icing time could make a great contribution to the theoretical and numerical droplet icing model on the hydrophobic surface. The effects of surface wettability, droplet diameter, surface temperature, droplet impact speed, and the inclined angle of surfaces will be experimentally investigated in detail. This study aims to find out a relationship or even correlation between total icing time and droplet oscillation time and the effect of the surface wettability, droplet diameters, the surface temperature, and the droplet impact speed. Specifically, this thesis will consider the droplet impact at different inclined angles to compare with the result on a flat surface. The droplet total oscillation time is defined as the time between the moment when the droplet first impacts on the surface and when the droplet becomes steady. The droplet total icing time is defined as the time measured from the moment when the droplet first impact on sample surface until it is fully frozen. The droplet total icing time and oscillation time will be studied to compare the hydrophobic surface machined by the conventional mechanical technique with the advancing chemical technique on an inclined surface. Specifically, the objectives are

- To provide a more detailed understanding of the surface wettability effect to the droplet dynamics and ice formation.
- To refine experimental methodology from the previous experiment based on literature review.
- To examine the relationship between the total icing time and the surface

wettability, droplet diameters, the impact velocity, and the inclined angle of the sample surface.

- To conduct dimensional analysis of the relationship between the total icing time and the Reynold number, Weber number, and f number.
- To examine the relationship between the droplet impact dynamics and the wettability, the droplet diameter, the impact velocity, and the inclined angle of the sample surface.
- To examine the gliding and roll off process on the inclined sample surface.

Chapter 2

Literature Review

2.0 Introduction

Chapter 2 contains a general literature review of basic and advanced knowledge on hydrophobicity, droplet dynamics, and droplet icing process on a solid surface. All the materials of literature review are related to this research topic. The basic knowledge of surface wettability is introduced and followed by metallic hydrophobic surface machining. The basic knowledge and modelling of droplet dynamics and ice formation process on the solid surface is reviewed. At the end of this chapter, the experimental methods for droplet dynamics and ice formation are reviewed to provide more thoughts for this research.

2.1 Surface Wettability

In 1964, superhydrophobic (lotus effect) phenomenon related to surface roughness was discovered by Dettre and Johnson. Subsequently, the unique hydrophobic properties of lotus leaves have become the main research area because of the fundamental interests in wetting and directional flow of water [14]. The lotus effect has various advantages such as water repellency, small flow resistance, and self-cleaning from any dirt. The contact angle was first brought up by Thomas Young in 1805, which means a unique contact angle of the droplet in a given three phase interfacial system under a given temperature and pressure [17].

$$\cos \theta = \frac{\gamma_{sv} - \gamma_{sl}}{\gamma_{lv}} \quad (1)$$

where γ_{sv} , γ_{lv} , and γ_{sl} represent the solid-vapor, liquid-vapor, and solid-liquid interfacial tension respectively. θ is defined as the static contact angle.

The static contact angle is measured through the liquid to determine surface wettability of a solid surface, which is the angle between a solid surface and three-phase contact line. θ_Y in Fig. 1 (a) represents static contact angle. It is determined by liquid surface tension, surface chemistry, and roughness. The dynamic contact angle (contact angle hysteresis) is also a key property to define the surface wettability and self-cleaning ability. It is the difference between advancing angle and receding angle when the solid surface is tilted, and the droplet starts to roll off [15-17]. Fig. 2 shows the advancing and receding angles of a droplet on a tilted surface. The dynamic contact angle is also called contact angle hysteresis, which is $\Delta\theta = \theta_a - \theta_r$. In our normal life, outside surface of most substances is hydrophilic since they are very easy to be wet. The property of the hydrophilic surface is that the static contact angle less than 90° . For the hydrophobic surface, it is not very easy to be wet and the static contact angle is larger than 90° . Superhydrophobic surface means highly hydrophobic, which is extremely difficult to wet the surface. The key properties of superhydrophobicity is the static contact angle of a water droplet sits on the surface exceeds 150° and the contact angle hysteresis is less than 10° . Table 1 shows the detailed surface type with the information of static contact angle and dynamic contact angle.

There are two models to describe how droplet sits on a rough surface, which is shown in Fig. 1 (c). One state is called Cassie-Baxter Model when droplet rests on top of the surface protrusion and leaves an air gap on the bottom. The Cassie-Baxter state,

Table 1: Different surface types with their water repellency and mobility.

Surface type	Static contact angle	Dynamic contact angle
Hydrophilic	$< 90^\circ$	$> 10^\circ$
Hydrophobic	$90 - 150^\circ$	$> 10^\circ$
Superhydrophobic	$> 150^\circ$	$< 10^\circ$

which considered as the key factor to achieve superhydrophobicity, has very high-water repellency and droplet mobility. It is defined as shown in Eq. (2).

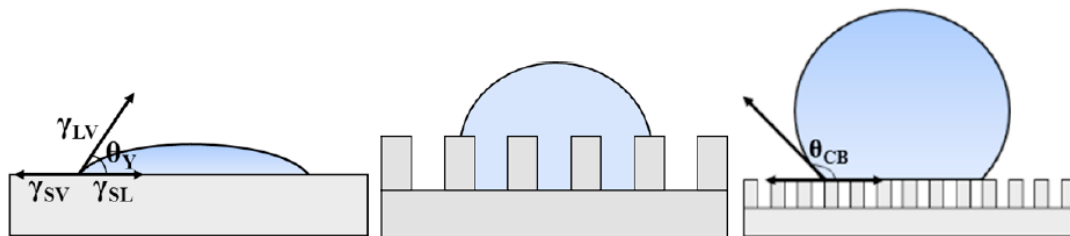
$$\cos \theta_{CB} = -1 + f(1 + r_f \cos \theta) \quad (2)$$

where r_f represents the roughness ratio of the wet surface area. f represents the fraction of the wet area by liquid.

The other model is the Wenzel model when droplet retains contact at all points with a structured surface which is shown in Fig. 1 (b). The Wenzel state is also called partially wetted state. Partial penetration into the rough surface is also called mixed region.

$$\cos \theta_w = r \cos \theta \quad (3)$$

where r represents the roughness ratio which is the ratio of actual area to the apparent area. θ_w represents the apparent contact angle at Wenzel state.



(a) Young's angle

(b) Wenzel state (wetting)

(c) Cassie-Baxter state

Figure 1: A droplet on a smooth or rough surface [20]

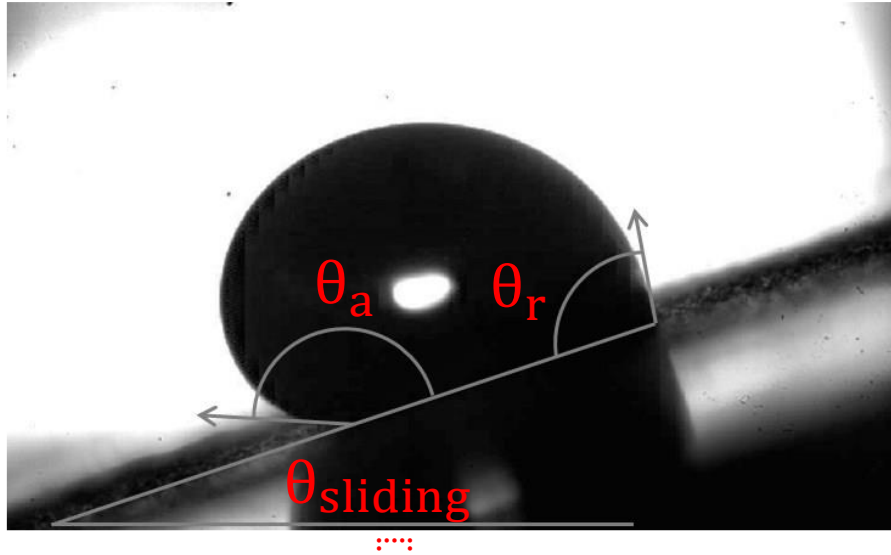


Figure 2: Advancing and receding angles of a droplet on the tilted surface [20]

Under the Wenzel state, the Cassie-Baxter equation shifts to Wenzel equation when $f = 1$ and $r_f = r$. The static contact angle is always larger in Cassie-Baxter state than Wenzel state, and Cassie state is what researchers want to achieve since it has the lowest wettability [17]. To improve Wenzel state to Cassie-Baxter state, contact angles can be increased by machining micro or Nano-structures to reduce the liquid-solid contact area, on the other hand, applying coatings with low surface energy can increase Young's contact angles. These two methods can be applied to develop a hydrophobic surface. It is essential to determine which state occurs during the experiment. The surface roughness is the key factor to improve the hydrophobic material to superhydrophobic. There are many designs of micro-structured surfaces to achieve superhydrophobicity, such as bricks, blades, honeycomb, and mushroom [12]. The surface wettability and the micro-structure plays an important role on droplet dynamics, wetting state, and icing time after the impact.

2.2 Metallic Hydrophobic Surface Fabrication

There are many mechanical ways to machine hydrophobic surfaces, such as wired

electrical discharge machine (WEDM), laser machining, sandblasting and micro-rolling [12-20]. Won [21-22] used wire electrical discharge machining technique to machine dual-scale structures on an aluminum substrate to achieve 156° static contact angle. The advantage of WEDM is that it only needs one-step process, and it is available to make the hierarchical structure with no additional treatment is required. The disadvantage is that only small scale of the workpiece can be fabricated. The laser irradiation is a more convenient and efficient technique to texture a metallic surface, but it still needs pretreatment. The laser technique is not good for curvature surface and pretreatment is required, such as chemical treatment and polishing [20]. Sandblast and solution immersion can also make microscale roughness, but they still need two-step fabrication process. Sandblast technique on the metallic surface can only achieve hydrophobic surface, and it is not a suitable technique to machine superhydrophobic surface compare with laser machining. There are also many designs of micro-structured surfaces to achieve hydrophobicity or even icephobicity, such as bricks, blades, honeycomb, and mushroom. Some doubly reentrant (hierarchical) structures can suspend any liquid even it has very low surface tension [23]. There are also many chemical ways to machine hydrophobic surface, such as chemical etching and electrodeposition. The chemical way is subtractive manufacturing process to either remove or add material in small scale to achieve hydrophobicity [24-25]. Li et al. [64] synthesized ZnO film on the metal surface to achieve micro or even nano-scale structure surface. Xiang et al. [65] used a electrodeposition method to add Zn-Ni on the mild steel to achieve certain roughness. The chemical method used to produce superhydrophobic surface in our group is zinc electrodeposition. Zinc electrodeposition is widely used for superhydrophobic surface due to corrosion resistance, commercial availability, and other characteristics. Two

main mechanical approaches are investigated to make a hydrophobic surface in our research, i.e., applying coatings with low surface energy and machining micro or nano-structures to reduce liquid-solid contact area. Recently, our research group has developed hydrophobic steel surfaces with micron-scale and sub-micron structures from laser fabrication and WEDM [20]. The surfaces achieved static contact angle higher than 120° . Surface roughness plays an important role in making hydrophobic and super-hydrophobic surfaces, and many designs have been investigated.

2.3 Droplet Dynamics on Hydrophobic Surfaces

The surface wettability is a key factor for droplet oscillation time and droplet icing time. The droplet impact dynamics on the hydrophobic and superhydrophobic surface also affects the droplet icing time since the droplet contact area varies during oscillation. Since early 1876, the experimental phenomenon of liquid droplet impact on solid surfaces has been attracting researchers based on droplet spreading and splashing analysis by Worthington [26]. Yarin [27] conducted a detailed review paper on the fluid dynamics of liquid droplet impact on both solid and liquid surfaces. The paper also explained different droplet impact phenomenon and analyzed droplet deposition, splashing, spreading and rebounding. The dynamics of a droplet on hydrophobic surfaces plays an important role in analyzing the heat transfer, ice nucleation, ice formation processes. In these days, extensive research has been focused on droplet dynamics on hydrophobic and superhydrophobic surfaces. The droplet impact dynamics has also been studied numerically with different computational fluid dynamics tools. Examples include the work of Harlow and Shannon [28], Trapaga et al. [29], Fukai et al. [30], Pasandideh-Fard et al. [31]. Shin et al. [32] simulated the three-dimensional impact of a droplet onto a solid surface

using the level contour reconstruction method, Sidik et al. [33] presented an atomistic–continuum hybrid method to investigate spreading dynamics of drops on solid surfaces. Guo et al. [34], Wu et al. [35] presented an atomistic–continuum hybrid method to investigate spreading dynamics of drops on solid surfaces.

$$\left[\frac{1}{4}(1 - \cos \theta) + 0.2 \frac{We^{0.83}}{Re^{0.33}} \right] \left(\frac{d_m}{D} \right)^3 - \left(\frac{We}{12} + 1 \right) \left(\frac{d_m}{D} \right) + \frac{2}{3} = 0 \quad (4)$$

where d_m is maximum spreading diameter, D_i is initial droplet diameter, θ is static contact angle of the surface. In addition, this equation has been modified by authors via experiments.

The dynamics of a droplet on hydrophobic surfaces plays an important role in analyzing the heat transfer, ice nucleation, ice formation processes. Scheller et al. [43] found that the ratio of maximum diameter to initial droplet diameter which is maximum spread factor $\xi = D_{max}/D$ is in the range of 1.25 to 5 in deposition scenario [57]. They created an empirical correlation [43]

$$\xi = 0.61 \cdot (Re^2 Oh)^{0.166} = 0.61 \left(\frac{We}{Oh} \right)^{0.166} \quad (5)$$

Bennett et al. [42] reviewed some of the theoretical models in detail. Scheller et al. [43] proposed a squeeze-flow model using a force balance to estimate the maximum spread. Mao et al. [44] developed a semi-empirical model to predict the maximum spread as a function of the Reynolds number (Re), the Weber number (We), and the static contact angle. Mohamed-Nabil et al. [45] investigated the droplet dynamics on a superhydrophobic surface. All interactions forces: forces exerted by the wall, either in the normal or the tangential direction and air drag force, between droplet and wall were considered. Bahadur et al. [46] develop a droplet impact dynamics model based on force balance between droplet inertial and the surface-tension-based retraction

force. By analyzing a droplet spreading on a hydrophobic surface via horizontal forces balance at the contact line. By applying Newton's second law of motion, neglect the shear stress in liquid, friction force on the surface and the air drag, the following governing equation for a droplet spreading on a hydrophobic surface can be developed:

$$m \frac{d^2 r}{dt_r^2} + 2\pi\sigma_{lv} (1-\cos\theta) = 0 \quad (6)$$

where m is the droplet mass, r is the radius of the droplet contacted with a surface, σ_{lv} is the surface tension of the liquid and θ is the contact angle of the droplet. In this governing equation, the first term is the droplet inertia or the resultant of force. The second term stands for the surface tension which acts radially inward. This governing equation has ignored any other resistant forces, for example, shear stress in the moving liquid and surface friction force. Also, equation (6) can be nondimensionalized as follows:

$$\frac{d^2 R}{dt^2} + \frac{1}{2}(1-\cos\theta)R = 0 \quad (7)$$

where $R = (r/r_{max})$, $t = (t_r/\tau)$, and $\tau = (m/4\pi\sigma)^{1/2}$. R is the dimensionless droplet radius at the contact line, t is the dimensionless spreading time, τ is a time dimensionless constant, and t_r is the spreading time.

Alizadeh et al. [47] investigated the droplets impact dynamics on plain and structured surfaces in a range of temperature from below freezing to near boiling conditions. Recently, Pattil et al. [48] investigated the droplet impact dynamics on micro-pillared hydrophobic surfaces experimentally. Pravinraj et al. [49] analyzed the drop dynamics on partial wetting surfaces by using lattice Boltzmann method and find out that with the progress of time the surface free energy decreases with increase in spreading area.

2.4 Ice Formation on Hydrophobic Surface

The theories for designing and developing a good hydrophobic surface or even icephobic surfaces cannot help to fully understand the dynamics, heat transfer and icing process of droplet impacts on the hydrophobic surface. In addition, the dynamics of a droplet on these surfaces plays an important role in analyzing the heat transfer, icing process, and ice adhesion. Surface with low wettability and surface energy plays a very important role in ice nucleation and ice adhesion. Extensive research focuses on anti-icing performance and ice removal on various superhydrophobic surfaces under different conditions. Kulinich et al. [50] investigated the shear stress required to remove the ice from the side on the superhydrophobic surface under various conditions. The group finds that the icephobic property of water-repellent surface deteriorates since the rough surface structure is worn during icing and deicing cycles. The water-repellent surfaces are not always ice repellent. The efficiency of icephobicity is significantly reduced in the high humidity since water condensation reduces the performance of hydrophobicity and increases ice adhesion on the water-repellent surfaces. Lower contact angle hysteresis reduces the force needed to detach the droplet on the surface. The contact angle hysteresis and size and structure of micro-groove plays an important role in ice adhesion theoretically, but they don't have any strong correlation [51]. Even for a superhydrophobic surface with strong water repellent ability, the ice adhesion may be strong if the droplet penetrates micro-grooves to achieve the Wenzel state or the micro-groove structure is small [52]. A broad range of geometries of water-repellent surfaces, such as micro-pillar, micro-mushroom, staggered bricks, posts and blades, are investigated by many researchers. Ice formation on the water-repellent surface is another topic that many researchers are interested in. Mishchenko et al. [12] found a transition zone of droplet

freezing around $-25\text{ }^{\circ}\text{C}$ to $-30\text{ }^{\circ}\text{C}$ on a superhydrophobic surface. Ice formed below this transition temperature can be easily removed. Bahadur et al. [2] established a one-dimensional heat transfer model on the superhydrophobic surface to predict the transient temperature distribution by solving two heat conduction equations in two different regions. Eq. 4 shows the equation which predicts the temperature at the liquid-solid interface. Ice nucleation submodel is also considered as heterogeneous ice nucleation at the liquid-solid interface and the free-energy barrier (ΔG) is also estimated by Fletcher [53].

$$T_{i\text{ n}\text{erface}} = T_{\text{droplet}} + (T_{\text{substrate}} - T_{\text{droplet}}) \frac{\text{erfc}\left(\frac{h}{2\sqrt{a_{ns}t_c}}\right)}{\text{erfc}\left(\frac{h}{2\sqrt{a_w t_c}}\right)} \quad (8)$$

where a_{ns} and a_w are thermal diffusivities of solid-air and water domain. t_c is the total time of the droplet in contact with the substrate.

By considering the ice crystallization mechanism, Jung et al. [54] observed that the ice nucleation starts from homogeneous nucleation instead of heterogeneous nucleation at the liquid-solid interface because of evaporation from outside of the droplet. The icephobicity is highly affected by micro-structure, humidity, temperature and environmental conditions.

By considering general heat conduction model of a single droplet and 1-D transient heat conduction equation, the general solution becomes:

$$T_L(x,t) = T_s + (T_{\text{droplet}} - T_s) \text{erf}\left(\frac{x}{2\sqrt{\alpha t}}\right) \quad (9)$$

where T_s is the temperature of the solid surface, and α is thermal diffusivity.

The assumptions are: (1) no convection between solid-air and liquid-air. (2) well insulated on the side. (3) Quasi-steady-state $T_L(\infty, t) = T_{\text{droplet}}$. With boundary and initial conditions as follows:

$$T(0, t) = T_s \quad (10)$$

$$T(\infty, t) = T_{droplet} \quad (11)$$

$$T(x, 0) = T_{droplet} \quad (12)$$

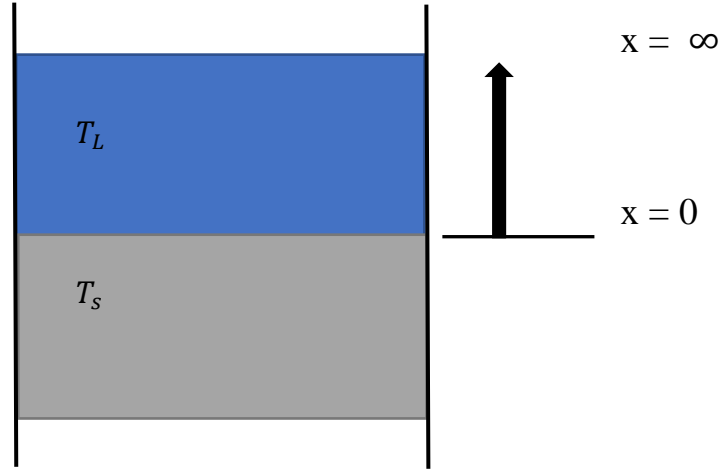


Figure 3: 1-D transient heat conduction model

The 1-D transient heat conduction model can be further expanded to model the heat transfer or even droplet icing on the hydrophobic surface in future work. Mishchenko et al. [46] created a heat transfer model and a droplet freezing model on the channel-like hydrophobic surface by expanding 1-D transient heat conduction model and classical heterogeneous nucleation theory.

2.5 Experimental Methods

2.5.1 Droplet Dynamics

The study of the droplet dynamics and the surface wettability is the main are focused by many researchers for a variety of applications. Extensive numerical and experimental techniques are generated and used to analyze droplet impingement on dry solid hydrophilic and hydrophobic surfaces. Based on various impact conditions, liquid properties, and surface wettability, Rioboo et al. [55] summarized six different

conditions of the droplet impact results. Fig. 3 shows the different droplet impact conditions which include deposition, prompt splash, corona splash, receding break-up, partial rebound, and complete rebound. From top to bottom droplet impact regime, the surface property varies from hydrophilicity to superhydrophobicity.

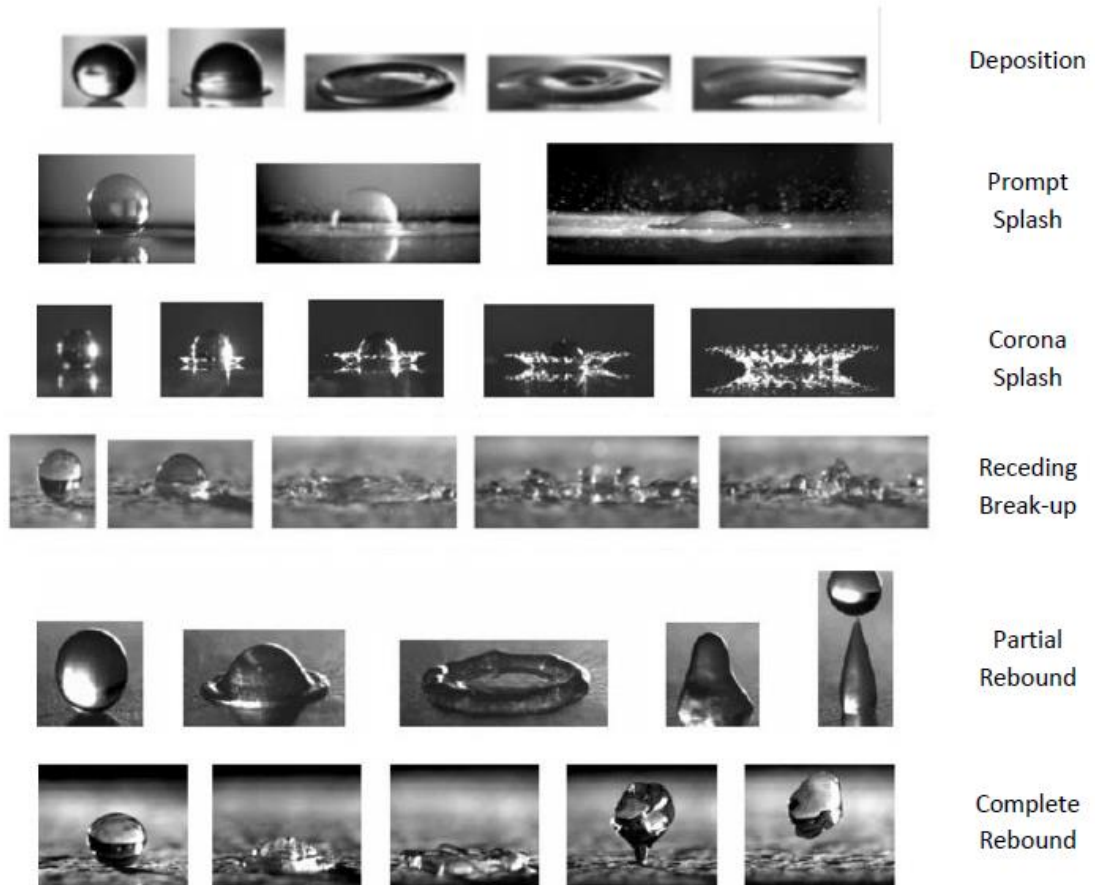


Figure 4: The various droplet impact conditions [27]

The droplet impact process includes four stages, the kinematic phase, spreading phase, relaxation phase and equilibrium phase. [56] The kinematic phase is a droplet falling process, which is not affected by the surface property. The spreading process comes right after kinematic phase. The droplet spreads to outside and forms a thin lamella until it reaches the largest spreading radius. During the spreading process, the inertia, viscosity, the surface tension and the surface wettability affects the spreading rate and the maximum spreading radius. The impact velocity and droplet diameter

increase the spreading rate, but inertia and surface tension reduces the spreading rate. The relaxation phase contains several spreading and retracting processes but spreading rate and radius decrease after each spreading process. The droplet becomes steady in the equilibrium phase. For droplet impacts on a superhydrophobic surface, the droplet doesn't partial rebound or complete rebound at low impact velocity. As the impact velocity increasing, bouncing in various forms occurs. Once a sufficiently high velocity is achieved to overcome the energy barrier, the droplet may penetrate into micro-grooves to form Wenzel state [57-58]. In deposition scenario, the droplet firstly spreads and then deposits on the surface. The smooth surface with high wettability normally belongs to deposition scenario without too much oscillation. The surface and liquid properties don't affect the radius of the droplet during the spreading and oscillating period, but the properties start to affect the droplet radius in actual deposition stage.

To analyze droplet dynamics by experimental method, a high-speed camera is needed to capture detailed and instantaneous droplet impact and spreading process. The droplet impact speed normally can be controlled by the height of droplet generation system based on gravity effect. A macro lens is also required to capture a very small droplet. Many kinds of droplet impinging systems are designed by different research groups to generate different droplet sizes and control droplet impact speed. Both front light or backlight techniques can be applied to capture droplet impact process. The dimension of droplet diameter and the solid-liquid contact diameter can be determined by the software of high-speed camera.

2.5.2 Droplet Icing Process

Nucleation of ice includes the heterogeneous nucleation and homogeneous

nucleation (spontaneous nucleation). Heterogeneous nucleation describes that nucleation of ice phase occurs on foreign particles such as the liquid-solid interface. Homogeneous nucleation describes ice phase initiated by water molecules only. The freezing point of the heterogeneous nucleation is significantly higher than homogeneous nucleation. [51] The critical free energy barrier must be overcome to meet the ice nucleation requirement. The equation of critical free energy barrier (ΔG^*) for a spherical cap is shown below.

$$\Delta G^* = \frac{8\pi\sigma_{12}^3}{3(\Delta G_v)} \cdot f(\eta, x) \quad (13)$$

where ΔG^* is a critical free energy barrier. σ_{12} is the surface free energy of the interface between 1 and 2. ΔG_v is the free energy difference for unit volume of two different phases. $f(\eta, x)$ is the geometrical factor.

The high-speed camera, macro lens, and droplet impinging system are also required to generate droplet and capture icing process. Sufficient light is required to capture the detail of the droplet [57]. Specific microscope connected with the high-speed camera is also used by many researchers to capture more detailed and clear icing process [57]. Fig. 4 shows a static droplet freezing process captured by a microscope connected with a high-speed camera. Artificial climate chamber is used for the most icing experiment to control environmental temperature, humidity, and air flow to meet researchers' requirements. The thermal electrical cooler and the thermal bath are also chosen to control the temperature of the sample surface and the droplet. Based droplet freezing on the superhydrophobic surface experiment, the ice accretion, ice adhesion and ice delay time are main research topics in recent years.

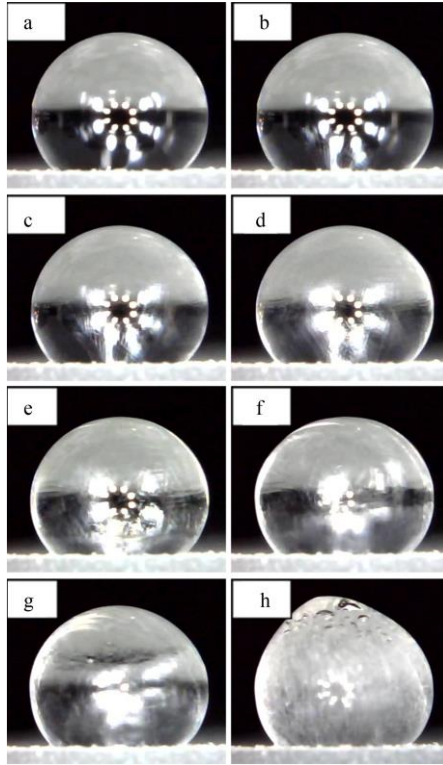


Figure 5: The freezing process of a static droplet on the superhydrophobic surface [57]

2.6 Summary

In chapter 2, the basic knowledge of surface wettability, the droplet dynamics and the droplet icing process are introduced. The modelling and previous experimental methods of droplet dynamics and ice formation process are also reviewed to prepare the more progressive experiment for this research topic. Chapter 3 introduces the methodology of this research, which includes the design of experiments (DOE), one-factor-at-a-time (OFAT), dimensional analysis, measurements of factors, experimental apparatus, experimental procedure, and sample design and fabrication.

Chapter 3

Methodology

3.0 Introduction

In this chapter, the design of experiments (DOE) technique, one factor at a time (OFAT) technique and the Design Expert software [7] (Version 8) are used to complete experiment design and data analysis. A two-level four-factor face-centered composite design (2^4) from the response surface methodology was used to exam the effects of four factors: surface temperature (A), impact speed (B), droplet temperature (C), and surface wettability (D) on the response of the droplet oscillation time. One factor at a time technique was used to analyze the effects of surface temperature, droplet impact speed, droplet diameter, and surface wettability to the droplet total icing time. The dimensionless variables which include Reynolds number (Re), Impact Weber number (We_i), f number and dimensionless time (t^*) are introduced to perform a dimensionless analysis. The experimental apparatus and procedure are also introduced in this chapter. Uncertainty analysis of different measurement equipment is explained in detail at the end of this chapter.

3.1 Design of Experiment Technique

The experiment designed and conducted by scientists is a series of tests to exam and evaluate the reasons for changes in the output responses while changing the factors of the experiment. The method selected to conduct an experiment is the key point to determine how factors affect the responses. The order and uncertainty to

conduct the experiment also play an important role when analyzing the responses. There are many different methodologies of experimentation, such as best guess approach, one-factor-at-a-time (OFAT) approach, and factorial approach. The one-factor-at-a-time approach is the most popular method that used by many engineers and scientists in research and industry area. The factorial design approach is more effective and accurate compared with the OFAT approach, since it can vary several factors simultaneously when studying two or more factors [59]. The OFAT approach has very limited ability to analyze the two or more factor interaction effects on the responses.

The more efficient and the economic approach to design and analyze the experiments is the design of experiments (DOE) methodology, which invented in the 1920's by Ronald A. Fisher. The analysis of variance (ANOVA) was investigated and statistics was firstly used in an experimental design by Ronald A. Fisher in 1918s [60]. The response surface methodology (RSM) was investigated in 1951 by George E. P. Box and widely used in quality improvement, product design, and uncertainty analysis [61]. Since a quadratic model may expect, the face-centered composite design (CCF) which is one type of method in response surface methodology was used to design and analyze the droplet oscillation time while impacting on a hydrophobic surface. By using the design of experiment method, it is clearer to know the process, significant factors, and mathematical model for predicting the experimental responses. In the modern years, the design of experiments has been widely used and successfully examined in many industries. It is much easier to use Design Expert to analyze the result with the application of design of experiment [62].

3.2 Determining the factors and levels

The aim of the study is to find out the significant factors and the corresponding effects to the droplet oscillation time or even icing time when impacting on a cooled hydrophilic and hydrophobic surface. A two-level four-factor face-centered composite design with 5 center points was selected for the design, and the run sheet is generated by Design Expert for conducting the experiment. The four factors were determined based on the initial guess on the significant factors. Based on the DOE experimental result, a few other design factors are considered such as the droplet diameter, impact speed, and inclined angle. The detail of factors and levels is shown in Table 2.

Table 2: Summary of design factors and levels

Factor	Name	Low Actual	High Actual	Low Coded	High Coded
A	Surface Temperature	-7 °C	-1 °C	-1	1
B	Height	2 cm	5 cm	-1	1
C	Droplet Temperature	5 °C	15 °C	-1	1
D	Surface Structure	N/A	N/A	NONE-SS	SS

Factor A is the surface temperature which is the temperatures of the structured (hydrophobic) and smooth (hydrophilic) surface for droplet impact experiment. The icing phenomenon is an important factor to oscillation time because the droplet would stop vibrating if it becomes ice. Since the droplet has a phase change phenomenon from liquid to solid ice, the surface temperature must be less than 0°C. The high level of factor A is -1 °C in order to make sure the droplet can fully become ice when the room temperature is high. The thermal bath with working fluid has a lowest operating limit, and the sample surface temperature is -7°C when the thermal bath working temperature is -15°C. The droplet can fully solidify when the temperature is in the

range of -7°C to -1°C.

Factor B is the height of the droplet travels, which is the distance between the tip of the capillary tube and the sample surface. The oscillation time is also affected by the potential energy of the droplet which is the distance of the droplet travels. If the height of the droplet is too large, the droplet would bounce off from the hydrophobic sample surface and no oscillation could be captured by the high-speed camera. The range of the height is determined based on the performance of the droplet oscillation and the high-speed camera.

Factor C is the droplet temperature. This is also an important factor for the droplet oscillation. The lower the initial droplet temperature, the faster it starts to solidify and stops vibrating. Since the droplet would solidify at 0°C, the initial temperature of the droplet should be higher than 0°C. The high level of factor C is room temperature which is 15°C.

Factor D is the surface structure of the sample which consists of structured surface (hydrophobic) and smooth surface (hydrophilic). This is one of the most important factors to the oscillation time because the droplet spreads and retracts more easily and frequently. Two sample surfaces were prepared. One is a hydrophilic surface with no micro-structured texture and the other one is a hydrophobic surface with micro-structured texture. Both sample surfaces are the same material which is 17-4 PH stainless steel.

The speed of the droplet when it first touches the metal surface is called the droplet impact speed (u). Neglecting the air drag force, the impact speed can be calculated from the distance (H_d) between the droplet generator needle tip and the metal surface. The impact speed is calculated based on Eq. 19 shown below.

$$u = \sqrt{2gH_d} \quad (14)$$

3.3 Dimensional Analysis

Dimensional analysis is to determine the relationships between different physical quantities. Based on the experimental parameters, the dimensional analysis is used to find out the relationship between the total icing time and a group of basic physical quantities such as temperature, the droplet impact velocity, droplet diameter, and the surface wettability. In the heat transfer scenario, various basic parameters are heat transfer coefficient, diameter, density, viscosity, thermal conductivity, and velocity. [63]

Table 3: Description of various parameters of heat transfer [63]

Variables	Description	SI Units	Dimensions
HTC	Heat Transfer Coefficient	$W/(m^2K)$	$MT^{-3}K^{-1}$
D	Diameter of the droplet	m	L
ρ_w	Density of water	kg/m^3	ML^{-3}
ρ_b	Density of bulk fluid	kg/m^3	ML^{-3}
μ_w	Dynamic viscosity of water	$Pa \cdot s$	$ML^{-1}T^{-1}$
μ_b	Dynamic viscosity of the bulk fluid	$Pa \cdot s$	$ML^{-1}T^{-1}$
k_b	Thermal conductivity of the bulk-fluid	$W/(m \cdot K)$	$MLT^{-3}K^{-1}$
k_w	Thermal conductivity of water	$W/(m \cdot K)$	$MLT^{-3}K^{-1}$
c_p	Specific heat	$J/(kg \cdot K)$	$L^2T^{-2}K^{-1}$
V	Characteristic velocity	m/s	LT^{-1}

The following dimensionless groups are used in analyzing the droplet dynamics and the total icing under different experimental conditions.

$$\text{Re} = \frac{\rho u D}{\mu} \quad (15)$$

$$\text{We} = \frac{\rho u^2 D}{\sigma} \quad (16)$$

$$\text{We}_i = \frac{\text{We}}{0.5 \cdot (1 - \cos \theta_a)} \quad (17)$$

$$t^* = \frac{t \cdot u_0}{D_0} \quad (18)$$

$$f = \frac{\cos \theta + 1}{\cos \theta_s + 1} \quad (19)$$

$$D^* = \frac{D}{D_0} \quad (20)$$

where ρ , u , D and μ are droplet density, impact velocity, initial impact diameter, and viscosity, respectively. σ is liquid surface tension. Re and We denote the Reynold number and the Weber number, respectively. f is the solid-liquid surface contact area fraction. The contact angle θ_s of a rough surface in equation 19 is assumed that the surface is composed of solid and air. With modification of Cassie and Baxter equation, the equation becomes $\cos \theta_s = f \cos \theta + (1 - f) \cos 180^\circ = f \cos \theta + f - 1$ [13]. θ_a is the advancing contact angle, and t^* represents the dimensionless time scale. θ is the static contact angle and θ_s is the static contact angle on the smooth surface with the same material. The average velocity of 0.77 m/s, 0.99 m/s, and 1.17 m/s is selected as u_0 , which is 0.98 m/s. The value of D_0 is determined as 2.82 mm, which is close to the diameter of a single droplet.

3.4 Measurement of the Factors and Responses

The factors and responses chosen for measurement were temperature ($^\circ\text{C}$), time (s), static contact angle ($^\circ$), and length (m). The handheld infrared camera is used to

measure the temperature of the droplet and the sample surface. Three measurements are taken by handheld infrared camera every time and the average value would be used. The height of the droplet is measured by micrometer every time from 2cm to 5cm. The response of the oscillation time and the icing time are measured by a high-speed camera. The camera is set from 600 frames per second to 2000 frames per second, and the oscillation time can be determined by the number of pictures taken by the high-speed camera during the vibration. The number of pictures taken by high-speed camera divided by frames per second is the oscillation time (s) or the total icing time (s). The diameter of the droplet is measured by the high-speed camera. The static contact angle is measured by the goniometer in the lab. Five measurements are taken by the goniometer for each sample surface and the average value is used in the future analysis. The total icing time can be measured and determined by looking at the recording time on the high-speed camera. The impact moment and completely frozen moment can be captured by the high-speed camera.

3.5 Experimental Apparatus

Figure 6 and 7 shows the apparatus for the liquid droplet impact and icing experiments. It consists of a stand (6, 7) (Fisher Scientific, Heavy Duty Support Stand) with a tilt base (1) (World Precision Instruments, Stand Tilting, M-3) of adjustable inclination angles, a cold plate (2) (AAVID Thermally, Hi-Contact 2-Pass Cold Plate) that is mounted on the tilt base and controls the temperature of sample surfaces (3), and a thermal electric cooler (4) (TE Technology, Thermoelectric Cold Plate Cooler) where a small copper tube (Sigma-Aldrich, Stainless steel capillary tubing 1/16 in) is buried for generating liquid droplet with controllable temperatures. To generate small water droplets, several needles of different inner diameters were used at the bottom

end of the drop generator tubing. The liquid comes from a syringe pump (Harvard, Syringe pump, MMP 3.3) which is not shown in this diagram, and the cold plate is connected to a thermal bath (Fisher Scientific, Thermal bath, ISO TEMP 6200) provides control of the surface temperature of the samples being tested. With this setup, we can test water droplets with controlled temperatures impacting on different metal surfaces at various angles and different temperatures. High-speed imaging investigations were conducted on droplet dynamics and icing phenomena with a high-speed camera (Vision Research, Phantom Camera, V611). The camera was connected to a laptop for video and picture captures. An LED light and light diffuser (Edmund Optics, Diffuser OPAL 50 mm) were used to provide light while capturing the droplet impact and icing process. The temperature of the sample surface and droplet is measured by an infrared camera (FLIR E60 Infrared Camera). The target parameters in this study, the droplet dynamics and total icing time can be determined from analyzing the images taken by the high-speed camera. The uncertainties of the equipment used during the experiment are shown in table 4. The uncertainties are obtained directly from equipment manuals and website to better understand the measured values of temperature, contact angle and total icing time. Based on the uncertainty table shown in table 4, the measured temperature of sample surface has the uncertainty of $\pm 2^{\circ}\text{C}$. The measured total icing time has the uncertainty of ± 20 ns from the high-speed camera. An additional error is also caused by human eye's inability to read the exact droplet fully frozen moment and exact measurements taken by the ruler and tape. The reasonable average uncertainty cause by the human reaction is around 0.5s. The measured height and droplet diameter have the uncertainty of ± 0.5 mm from measure tape and ruler. The error bar will not be shown in the figures in later results and analysis chapter to keep the figure clearer.

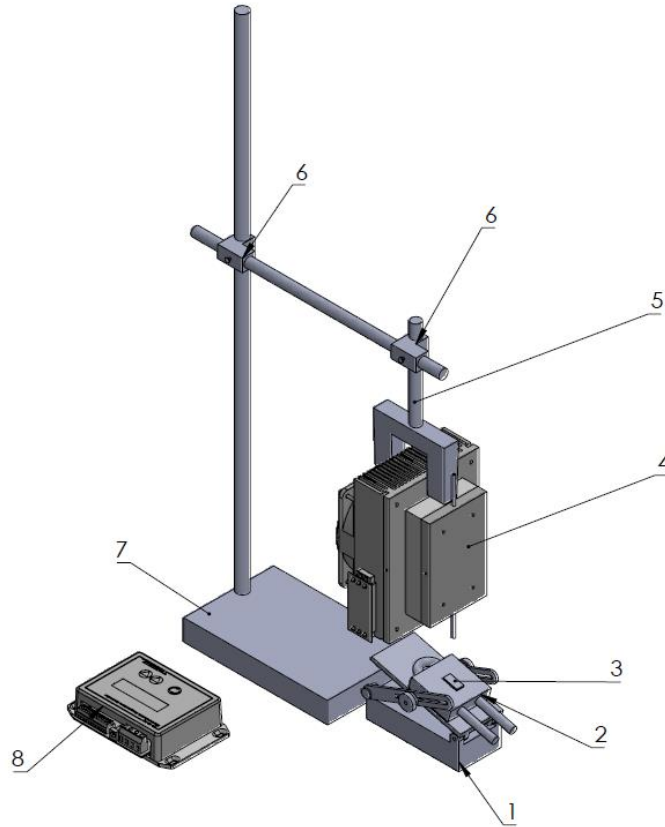


Figure 6: Liquid droplet impact and icing apparatus

Table 4: The uncertainty table of the equipment used in the experiment

Equipment	Operating Range	Uncertainty
Thermal Electric Cooler	-20 to 80°C	± 0.1°C
FLIR E60 Infrared Camera	-20 to 650°C	± 2°C
Isotemp Heated Bath Circulators	-25 to 200°C	± 0.01°C
Measure Tape	MAX 25'	± 0.5 mm
Measure Ruler	MAX 15 cm	± 0.5 mm
High-Speed Camera	MAX 6242 fps with full resolution	± 20 ns
Human Eye		±500 ms

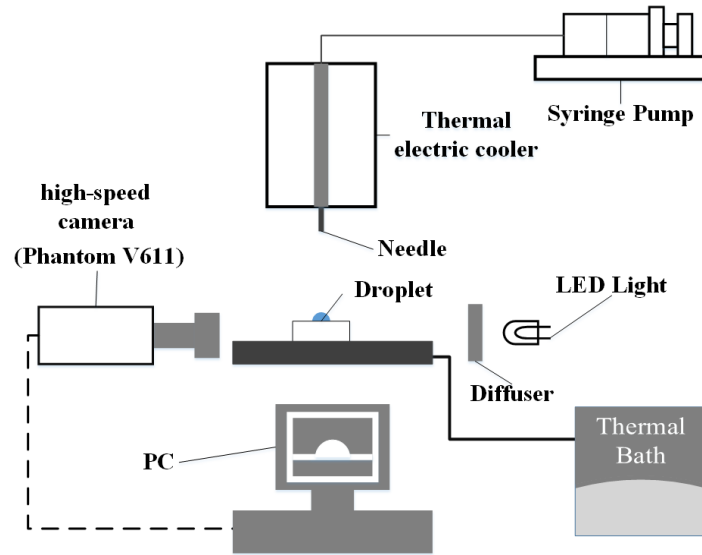


Figure 7: Experimental systems of droplet impact and icing

3.6 Sample preparation

Several machined and coated sample surfaces with various wettabilities were used in the experiments. The static contact angle and dynamic contact angle of each sample surface were measured by a contact angle instrument (Dataphysics, OCA 15EC). Five measurements were conducted for each sample and the average value was used in further analysis. Table 5 and 6 shows the measured static and dynamic contact angles of all sample surfaces. The contact angles of various samples are between 77° and 145° , which include the hydrophilic and the hydrophobic surfaces. The typical uncertainty for any given droplet measurement is around $\pm 1^\circ$, but the spread of uncertainty is around 10° for several droplets. The uncertainty of each sample is calculated based on the equation used in Cui's paper [20].

The material is stainless steel (17-4 PH) for all samples. The smooth sample was as received with no mechanical machining or coating. Channel 1 is a 20×20 mm machined surface by the wired electrical discharge machining. WEDM where a wire is used as an electrode to cut metal into designed structures using a programmed wire

path. The high potential difference is generated between the wire and the metal under a dielectric liquid. When the wire approaches the workpiece, the electrical discharge is converted into heat and melts the metal. Fig. 8 clearly illustrates the WEDM process

Table 5: Static contact angle of different sample surfaces

Run Number	Static Contact Angle (°)						
	Smooth	Channel 1	Channel 2	Coated channel 1	Varied channel	Coated channel 2	Coated varied channel
1	77	107	124	128	130	137	144
2	77	112	125	128	128	140	145
3	79	113	123	128	132	140	145
4	77	114	122	127	131	138	144
5	75	111	123	127	129	139	147
6	76	112	125	128	129	140	145
Average	77±3°	112±5°	124±5°	128±5°	130±5°	139±5°	145±4°

Table 6: Advancing and receding contact angles of different sample surfaces

Sample Surfaces	Advancing Contact Angle (°)	Receding Contact Angle (°)	Hysteresis (°)
Smooth	88±3°	51±3°	36±3°
Channel 1	132±5°	104±5°	27±5°
Coated Channel 1	135±5°	103±5°	31±5°
Channel 2	123±5°	84±5°	38±5°
Coated Channel 2	149±5°	129±5°	20±5°
Varied Channel	149±5°	129±5°	20±5°
Coated Varied Channel	150±4°	129±4°	21±4°

and a waveform of a voltage applied. The detail size of microstructure on channel 1 is shown in Fig. 9 (a). The samples of channel 2 and varied channel, shown in Fig. 9 (b) and (c) respectively, are 30×20 mm surfaces fabricated with laser machining [20]. The high-power laser beams are used to create sub-micron channels and some hierarchical multiscale surface structures under a certain designed path. The detail drawings of channel 2 and varied channels are shown in Fig. 9 (b) and 9 (c). Samples of these 3 designs were also coated with a low surface energy material to further increase surface hydrophobicity. The coating used for the samples was a Metal Repellency Treatment coating from Aculon, a company commercializes unique surface and

interfacial materials [20]. The coating was tested and applied to the machined surfaces to significantly increase the contact angle and hysteresis. One extra superhydrophobic sample made by electrodeposition method was also tested for droplet dynamics on an inclined surface. 1:0.2M zinc chloride and 3.5M ammonium chloride were used to the composite electrolyte and stearic acid was coated on the sample surface to achieve low surface energy on stainless steel. The channel 2 and varied channel sample surfaces were machined by Cui [20]. The electrodeposition sample was machined by Boyang Gao in our group from the chemistry department.

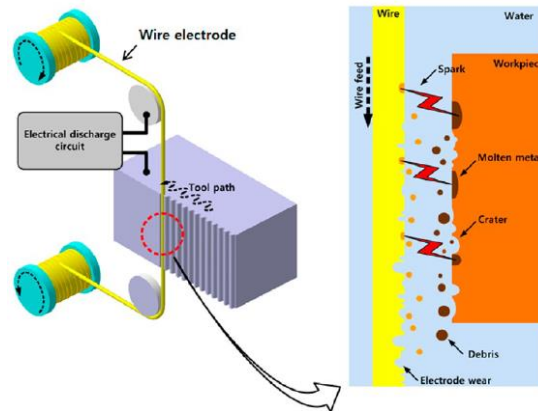


Figure 8: Schematic diagram of WEDM process [21]

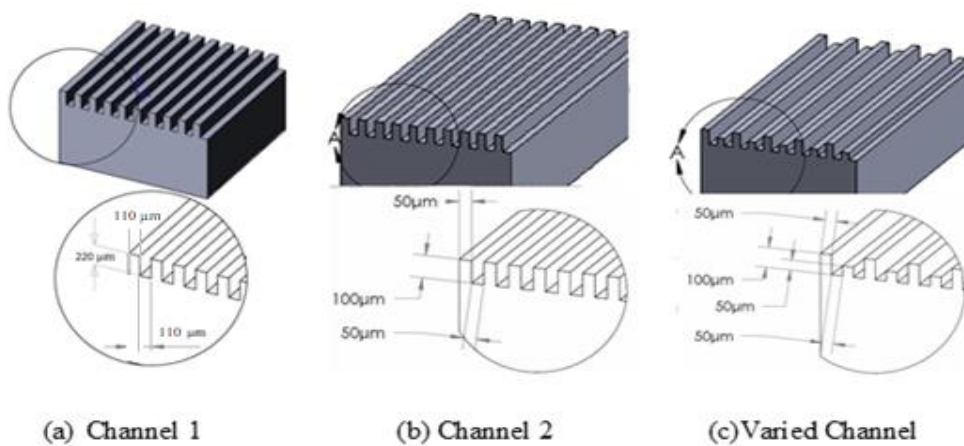


Figure 9: Detail drawings of Channel 1, Channel 2 and varied channel

3.7 Experimental Procedure

The DOE technique was used to determine the effect of surface temperature, impact velocity, droplet temperature, and the surface wettability on the droplet oscillation time. The experiment setup was well organized and properly installed to prevent any unacceptable errors. The measurement was taken care by reliable device each run to make sure accuracy of each factor and response. A two-level four-factor face-centered composite design with five center points was chosen for this experiment, and factors with levels were entered into Design Expert to generate the run sheet. There are total 38 runs in this experiment. The run sheet was randomly generated and the experiment was conducted followed the order of run sheet. The detailed run sheet includes the results is shown in Table 5. The experiment was finished randomly within one day, so there is no blocking and hard to change factor effect.

One factor at a time (OFAT) technique was used to investigate the effect of surface temperature, droplet impact velocity, impact inclined angle, droplet diameter, and surface wettability on droplet total icing time. The droplet total icing time is defined as the time measured from the moment when the droplet first impact on sample surface until it is fully frozen. The part (b) in Fig. 23 is the starting moment when the droplet first impact on the sample surface and the part (l) is the endpoint which the droplet is completely frozen.

Table 7: Detailed run sheet and experimental results

Std	Run	Factor 1 A: Surface Temperature C	Factor 2 B: Impact speed m/s	Factor 3 C: Droplet Temperature C	Factor 4 D: Surface Wettability	Response 1 Oscillation Time s
8	1	-5.00	1.00	15.00	None-SS	0.028
10	2	-5.00	0.81	10.00	None-SS	0.037
6	3	-5.00	0.63	15.00	None-SS	0.035
36	4	-10.00	0.81	10.00	SS	0.095
2	5	-5.00	0.63	5.00	None-SS	0.047
17	6	-10.00	0.81	10.00	None-SS	0.058
22	7	-15.00	1.00	5.00	SS	0.048
35	8	-10.00	0.81	10.00	SS	0.112
20	9	-15.00	0.63	5.00	SS	0.062
13	10	-10.00	0.81	5.00	None-SS	0.048
19	11	-10.00	0.81	10.00	None-SS	0.047
33	12	-10.00	0.81	15.00	SS	0.077
29	13	-5.00	0.81	10.00	SS	0.073
38	14	-10.00	0.81	10.00	SS	0.16
3	15	-15.00	1.00	5.00	None-SS	0.045
34	16	-10.00	0.81	10.00	SS	0.11
27	17	-5.00	1.00	15.00	SS	0.088
31	18	-10.00	1.00	10.00	SS	0.042
24	19	-15.00	0.63	15.00	SS	0.205
14	20	-10.00	0.81	15.00	None-SS	0.042
28	21	-15.00	0.81	10.00	SS	0.081
30	22	-10.00	0.63	10.00	SS	0.113
7	23	-15.00	1.00	15.00	None-SS	0.035
26	24	-15.00	1.00	15.00	SS	0.078
23	25	-5.00	1.00	5.00	SS	0.123
25	26	-5.00	0.63	15.00	SS	0.158
12	27	-10.00	1.00	10.00	None-SS	0.033
18	28	-10.00	0.81	10.00	None-SS	0.038
1	29	-15.00	0.63	5.00	None-SS	0.04
11	30	-10.00	0.63	10.00	None-SS	0.067
9	31	-15.00	0.81	10.00	None-SS	0.037
4	32	-5.00	1.00	5.00	None-SS	0.035
37	33	-10.00	0.81	10.00	SS	0.11
5	34	-15.00	0.63	15.00	None-SS	0.06
15	35	-10.00	0.81	10.00	None-SS	0.04
16	36	-10.00	0.81	10.00	None-SS	0.03
32	37	-10.00	0.81	5.00	SS	0.09
21	38	-5.00	0.63	5.00	SS	0.16

3.8 Summary

In chapter 3, the design of experiments and one-factor-at-a-time experimental technique are used and introduced for my experiment. The experimental apparatus and procedure are well organized to reduce the uncertainties. The uncertainty analysis and sample preparation are also introduced at the end of chapter 3. The experimental results and analysis will be presented in chapter 4.

Chapter 4

Results and Analysis

4.0 Introduction

In this chapter, ANOVA analysis is applied to analyze the relationship between the droplet oscillation time and four factors which are surface temperature, droplet impact speed, droplet temperature and the surface wettability. Dimensional and non-dimensional analysis are used to determine how surface temperature, droplet impact speed, droplet diameter, and surface wettability affect droplet dynamics and ice formation on both flat and inclined surface. The sample surface generated by using electrodeposition method is also tested on the inclined surface and captured using the high-speed camera. Some results in this chapter are in agreement with previous work done by other researchers, and many results are very new and haven't done by any other researchers yet.

4.1 Droplet Oscillation time

ANOVA is a powerful tool in DOE which is an acronym stands for analysis of variance. It is very useful to test for differences between more than two population means or multi-factors. P value in ANOVA table is used to determine if the factor is significant based on null hypothesis. An ANOVA table was generated by Design Expert after completing a total of 38 runs of experiments. The results in Table 8 shows the following significant factors: the impact speed, the surface wettability, the interaction effects between surface temperature and droplet temperature, and the

interaction effects between surface temperature and surface wettability since their p-values are all less than 0.05.

Table 8: ANOVA results

Source	Sum of Squares	df	Mean Square	F Value	P-value
Model	34.72	10	3.47	14.97	<0.0001
A-Surface Temp.	0.031	1	0.031	0.13	0.7191
B-Impact speed	4.06	1	4.06	17.49	0.0003
C-Droplet Temp.	0.019	1	0.019	0.082	0.7768
D-Surface Wett.	26.68	1	26.68	115.01	<0.0001
AB	0.00769	1	0.00769	0.033	0.857
AC	1.53	1	1.53	6.61	0.0160
AD	1.28	1	1.28	5.51	0.0264
BC	0.49	1	0.49	2.11	0.1579
BD	0.054	1	0.054	0.23	0.6320
CD	0.58	1	0.58	2.49	0.1259
Residual	6.26	27	0.23		
Lack of Fit	4.50	19	0.24	1.07	0.4880
Pure Error	1.77	8	0.22		
Cor Total	40.99	37			

A droplet experiences impact, spreading and retraction phases on the surface. Fig. 10 shows a series of images of a droplet with interesting variations of droplet shapes impacts on the hydrophilic surface with the impact speed equal to 0.77 m/s at the room temperature. The droplet moves into spreading phase after impacting on the surface and lasts about 6 ms. The retraction phase begins after the spreading phase. The horizontal and vertical scales of the droplet vary during the spreading and retraction phases. The droplet becomes steady after many cycles of the droplet vibration, and the kinetic energy converts to the surface energy, internal kinetic energy of the droplet and the internal energy [66]. There is also energy dissipation by viscous

forces, frictions and air drags.

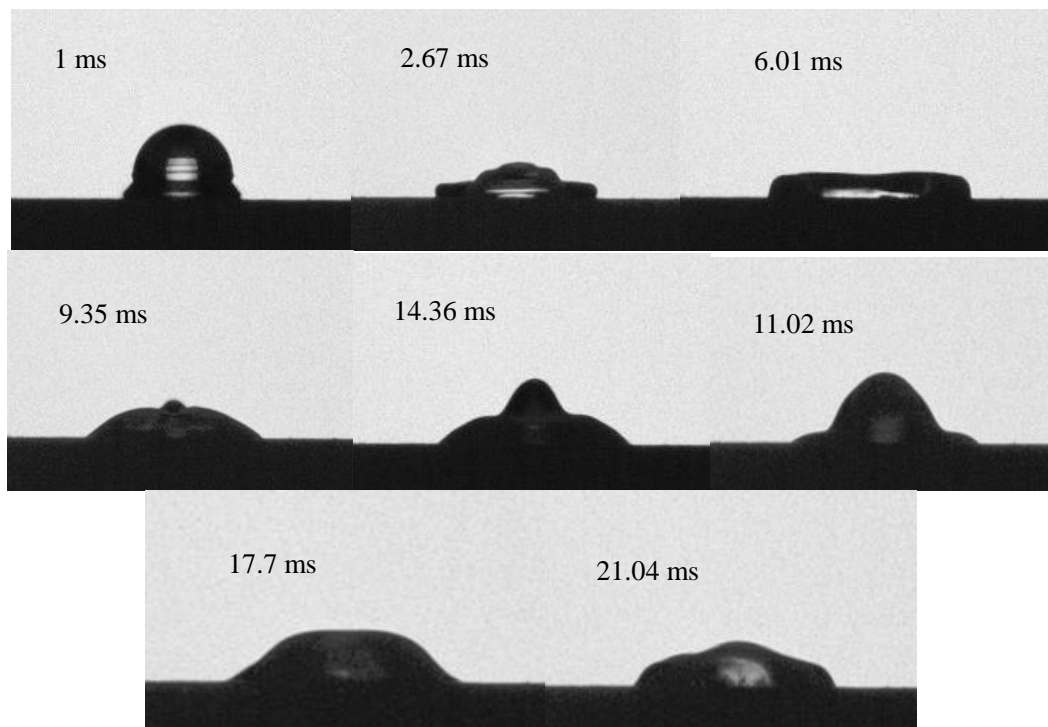


Figure 10: Droplet (with impact speed = 0.77 m/s) oscillation on the surface of the hydrophilic sample. Surface and droplet temperatures are at room temperature of 18.5 °C.

The ANOVA analysis shows a desirable and reasonable design model has been created. The diagnostic plots should be proceeded to make sure the assumptions are valid. The assumptions for the DOE model are: (1) The experiment data is normally distributed. (2) The experiment data has constant variance. (3) All data is independent of each other. (4) Random order experiment. Fig. 11 to 15 are residuals plot based on experimental data and result predicted by DOE model to determine if the DOE model is valid. Fig. 11 shows a normal plot of all residuals. The results clearly shows that all data points are distributed around a straight line, which means that the two-level four-factor face-centered composite design model adequacy is good and experiment data follows the normal distribution. Fig. 12 and 13 indicates that all the residual points are uniformly distributed around the middle line when the externally studentized residuals are zero and within the outside boundaries which means the

variance is constant. Fig. 14 shows that the predicted values based on the model are very close to the actual values from the experiments. The Box-Cox normality plot is widely used in DOE model. Most statistical tests are based on the assumption of normality of samples. The assumption of normality often makes the DOE tests that are simple, mathematically tractable, and powerful compared to tests that do not make the assumption. However, many samples are not approximately normal, so an appropriate transformation of a data set can achieve normality based on the Box-Cox plot. As seen from the Box-Cox plot, it suggests an inverse square root transformation for the design model which means $\lambda = -0.5$. As Design Expert suggests, an inverse square root transformation is selected for the model.

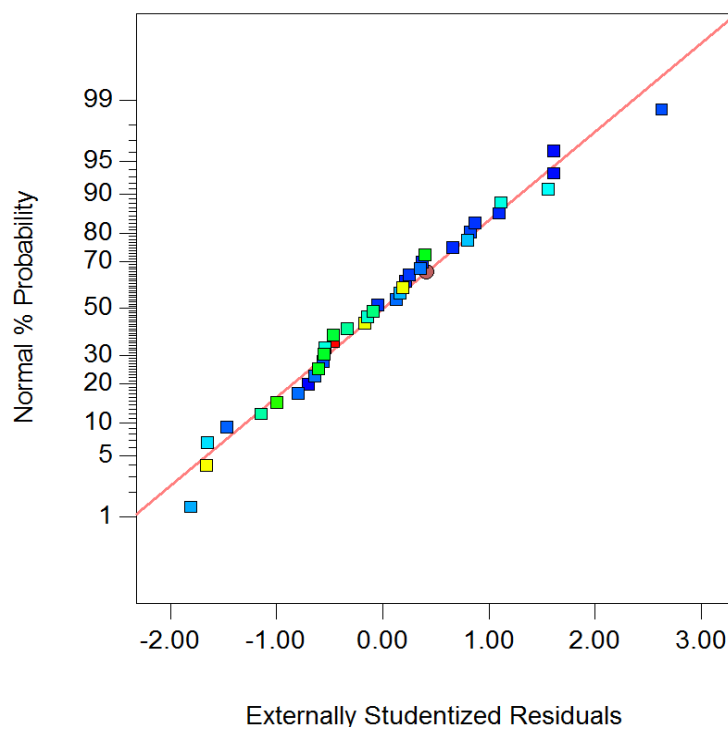


Figure 11: Normal plot of residuals

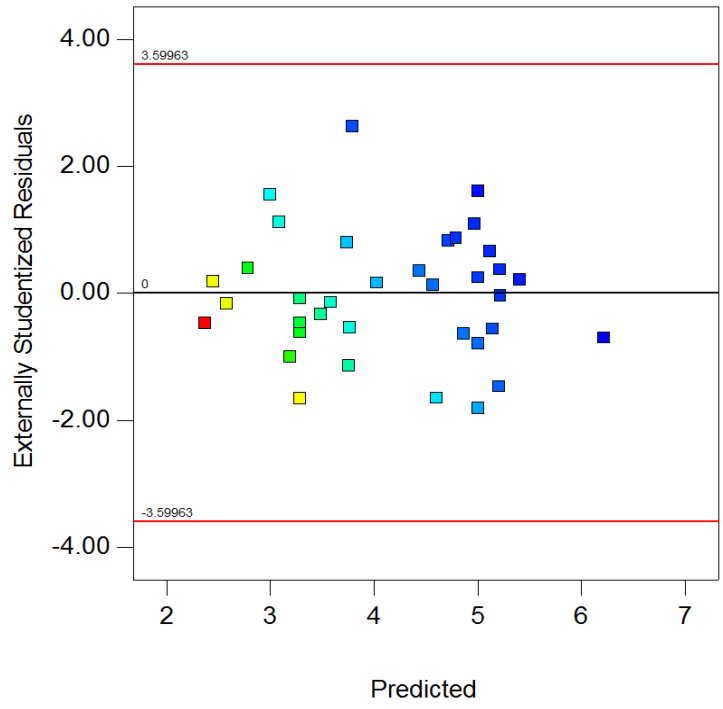


Figure 12: Residuals vs. predicted

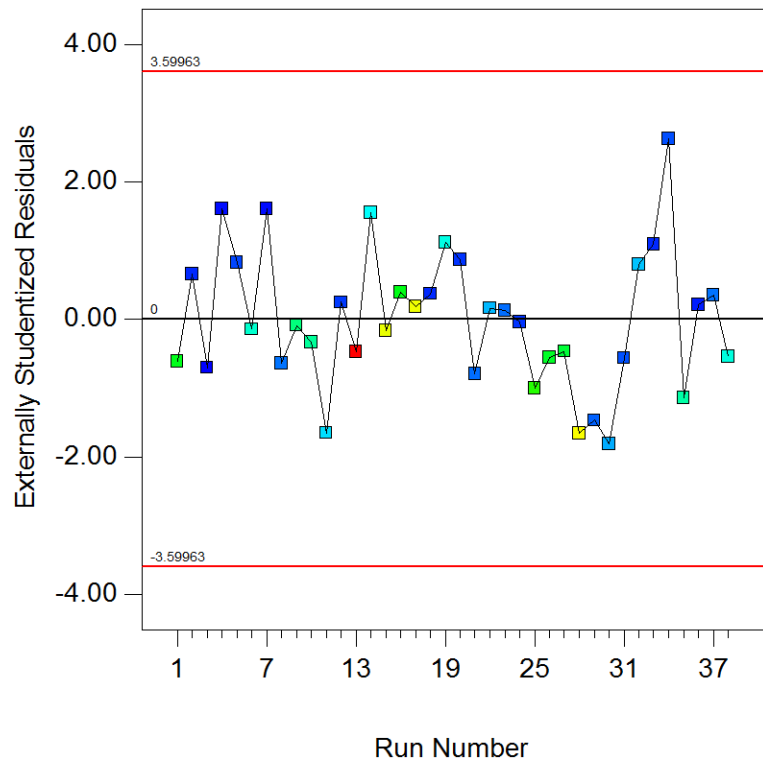


Figure 13: Residuals vs. run

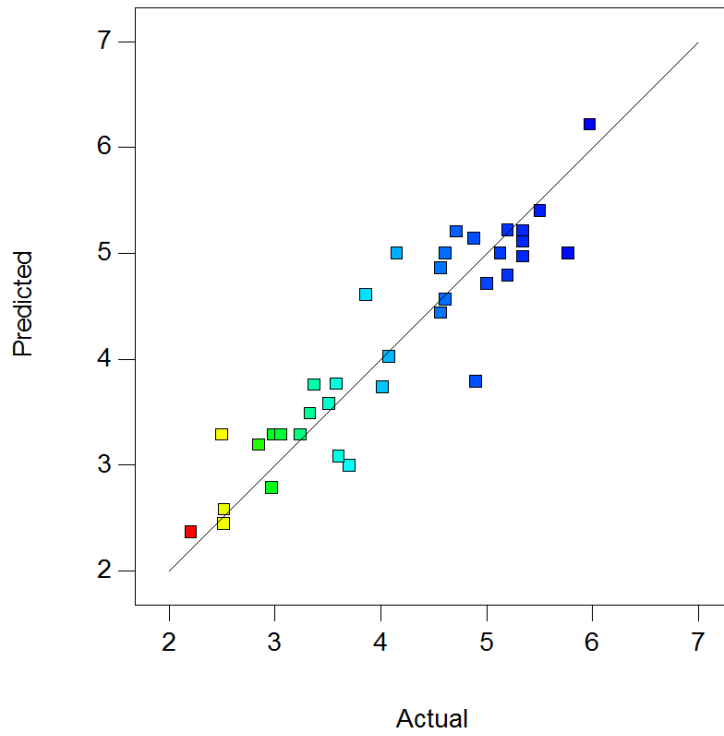


Figure 14: Predicted result vs. actual experimental result

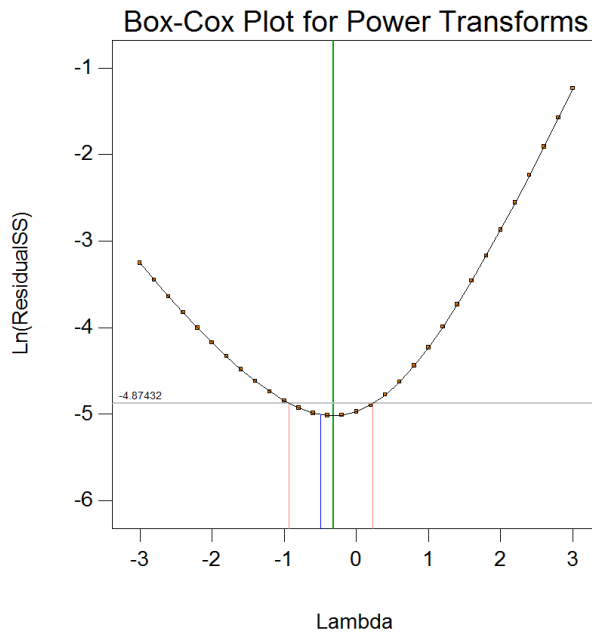


Figure 15: Box-Cox plot for power transformations

DOE methods were used to analyze the effects of operational factors. Fig. 16 indicates that the oscillation time increases as the droplet temperature increases on a hydrophobic surface since the green solid line has an inclined slope when the static

contact angle is 120° and flatter horizontal line for the hydrophilic surface. The oscillation time doesn't change much with temperature on the hydrophilic surface. The viscosity of the droplet increases while decreasing the droplet temperature, so the viscous dissipation loss increases during the spreading and retracting phase. The total droplet oscillation time decreases with the higher surface wettability or lower droplet temperature since higher viscous dissipation loss. The droplet temperature doesn't affect the total droplet oscillation time much on the hydrophilic surface may due to the surface roughness and surface wettability. Fig. 17 shows that higher surface temperature leads to increase of oscillation time for a hydrophobic surface, and it doesn't affect the oscillation time on hydrophilic surfaces. The dotted green and red lines represent the 95 percent confidence band in the prediction for any given factor level.

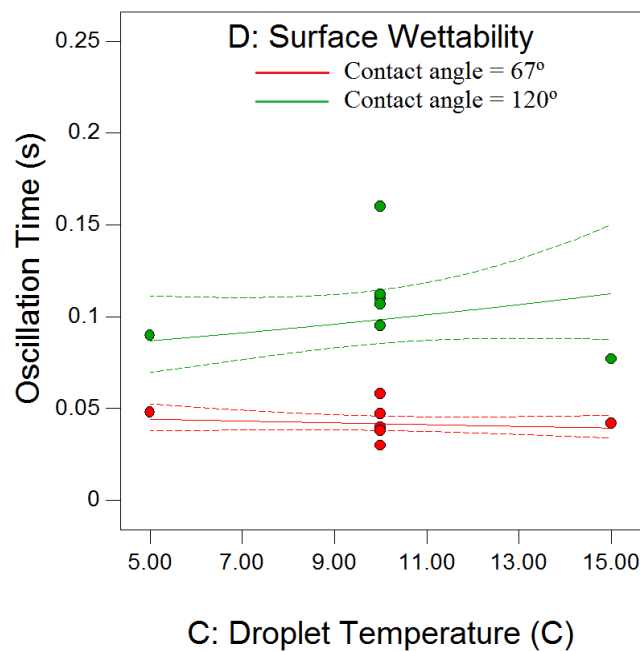


Figure 16: The interaction plot between droplet temperature and surface wettability. The graph is plotted under surface temperature = -10°C and impact speed = 0.81 m/s .

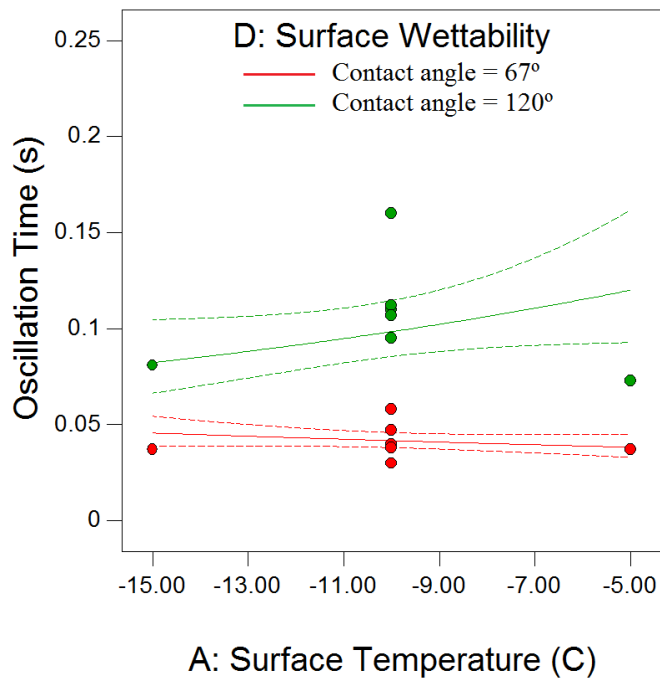


Figure 17: The interaction plot between surface temperature and surface wettability. The graph is plotted under droplet temperature = 10 °C and impact speed = 0.81 m/s.

Fig. 18 shows that the oscillation time is longer on a hydrophobic surface than a hydrophilic surface under the same impact speed and temperature. As the impact speed decreases, the oscillation time increases for both hydrophobic and hydrophilic surfaces. This occurs because the higher impact speed leads to a larger spreading area, and results in a faster temperature decrease. The viscous force and friction force dissipation is higher due to the faster impact speed. This result is more reasonable after considering the icing with the droplet spreading together. Fig. 19 shows images of droplets with different impact speed but at approximately the same time of 1ms after impact. It clearly shows that a higher impact speed leads to less oscillation time. The reason is that the larger spreading area results from a higher impact speed that creates greater contact area with a solid base, and the total freezing time is significantly decreased.

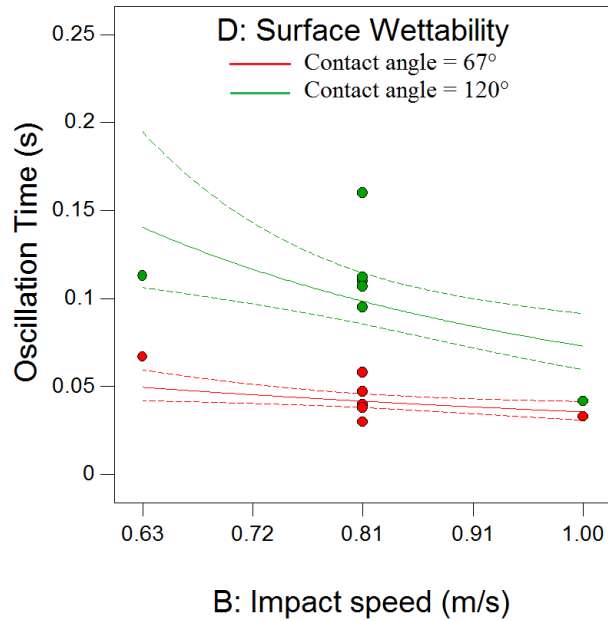


Figure 18: The interaction plot between impact speed and surface wettability. The graph is plotted under surface temperature = $-10\text{ }^{\circ}\text{C}$ and droplet temperature = $10\text{ }^{\circ}\text{C}$.

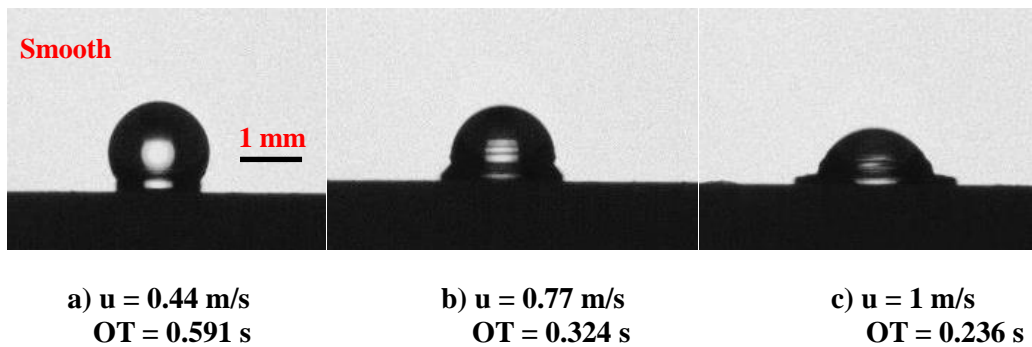


Figure 19: The droplet impact on the 17-4 PH stainless steel sample under different impact speeds. Surface and droplet temperatures are at a room temperature of $18.5\text{ }^{\circ}\text{C}$, and the diameter of the droplet is 1.80 mm.

Initial nominal diameters of the droplets are in the range of 2 mm to 5 mm. To analyze droplet geometry variations on the surfaces, the lateral and vertical dimensions of a droplet are defined as $2a$ and b , as shown in Fig. 20. Droplet dynamics can be studied by analyzing these geometrical parameters, as shown in Fig. 21. In the first few milli-seconds ($<10\text{ ms}$), the droplet experienced a fast-spreading process, indicated by increasing lateral dimension (a) and decreasing vertical dimension (b). Then there is a retraction process indicated by the shrinking of the lateral dimension and increasing vertical dimension. This oscillation repeats for

several cycles but with rapidly dampening amplitude until the droplet becomes steady and freezes in low-temperature cases.

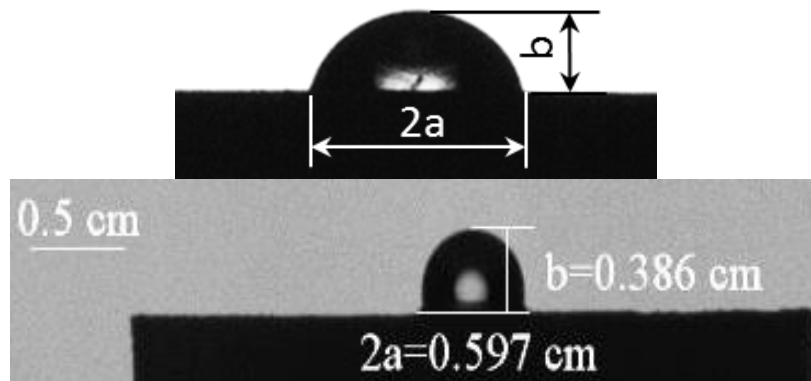


Figure 20: Droplet geometry and imaging scale

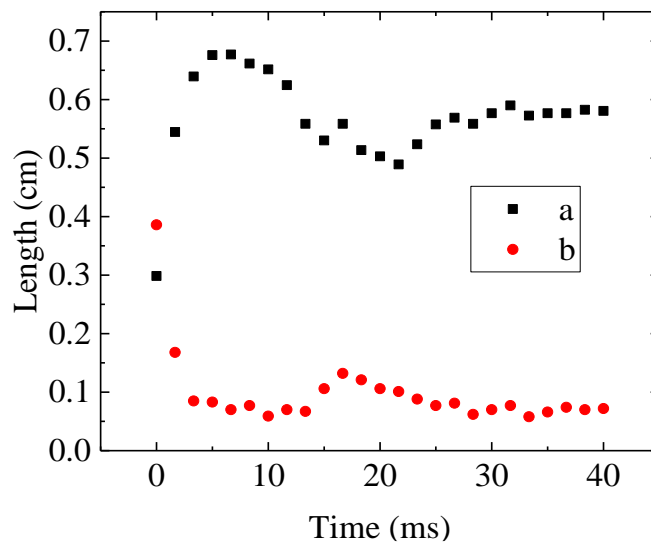


Figure 21: Droplet oscillations on the hydrophilic stainless-steel surface, with droplet initial temperature 18.5 °C, impact speed 1 m/s, steel surface temperature -7 °C.

4.2 Droplet Impact and Ice Formation Process on Flat Surfaces

The one factor at a time technique was used to investigate the effect of surface temperature, droplet impact speed, droplet diameter, impact inclined angle, and surface wettability on droplet total icing time. The droplet total icing time is defined as the time measured from the moment when the droplet first impact on sample surface until it is fully frozen. The temperature, relative humidity, and air pressure in the laboratory were kept constant during the experiment. Droplet dynamics and icing

experiments on flat surfaces were conducted under different conditions. The temperatures of the sample surfaces were varied from -10°C to -13°C . The droplet diameters were 1.80 mm, 2.82 mm, and 4.11 mm. The droplet impact speeds were changed from 0.77 m/s, 0.99 m/s, to 1.17 m/s. The droplet initial temperature was kept at 5°C . Surfaces with different wettabilities were studied, varying from the hydrophilic surface (the smooth stainless-steel sample) to the hydrophobic surfaces (textured stainless-steel samples). The surface condensation occurred during the experiment, and it coincides to the real environmental situation, so the condensation was not mitigated in purpose.

To better describe the dynamics of the moving droplet after impacting the flat surface, a coordinate system is shown in Fig. 22. The moment when the water droplet first impacts the sample surface is named as the impact point. The x-axis is parallel to the sample surface and y-axis is perpendicular to it, and the origin sits in the center of the droplet. Fig. 23 clearly indicates the typical droplet impact and icing process on a flat smooth surface. Kinetic energy, surface tension, air drag, liquid viscosity, and surface structure play important roles during droplet impact dynamics process. The surface temperature, droplet size, and the surface wettability play important roles on droplet icing process. In general, the water droplet moves into dynamic phase after impacting the sample surface, and the icing nucleation phase (phase change) occurs after the dynamic phase. The dynamic phase contains spreading phase (Fig. 23 b-e), retraction phase (Fig. 23 f-i), and relaxation phase which contains many cycles of spreading and retraction processes. The dynamic phase lasted 334 ms before moving into ice nucleation phase. The impact process of a water droplet ($D_i = 2.82$ mm) on the smooth sample surface at the temperature of -10°C and impact speed at 0.77 m/s is shown in Fig. 23. After the droplet impacts on the sample surface, a lamella was formed

from the base of the water droplet, and then a ring was formed which means the most volume of droplet stayed in the outside ring instead of inside lamella (Fig. 23 b-e). At the end of the spreading phase, the water droplet reached to its maximum contact diameter which is 5.31 mm (Fig. 23 e). During the spreading phase, the initial kinetic energy of the impinging water droplet was transferred to surface energy, internal energy, and kinetic energy inside the droplet [66]. The total spreading process lasted for 8 ms on the smooth surface. The retraction phase started right after the spreading phase (Fig. 23 f-i). During the retraction phase, the water droplet started to recoil from outside ring to the inside lamella. After relaxation phase which contained number cycles of spreading and retraction phases, the droplet becomes steady and reached its equilibrium state at around 334 ms. Ice nucleation started after the dynamic phase, and the water droplet took about 12.90 s to freeze. The droplet freezing process initiated at the liquid-solid interface (Fig. 23 j), and it propagated to the top of the droplet (Fig. 23 k). A small tip was formed on the top of the droplet at the end of the icing process (Fig. 23 l). A pointy tip is formed when the droplet is completely frozen because the water droplet expands during the freezing process. The combination of water expansion and surface tension on a spherical cap of the remaining liquid causes the small tip formation [30].

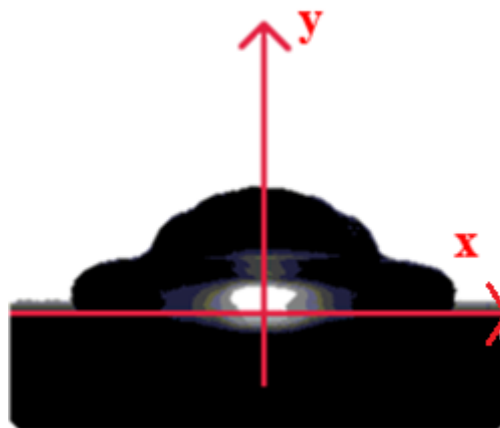


Figure 22: A coordinate system of droplet impact movement

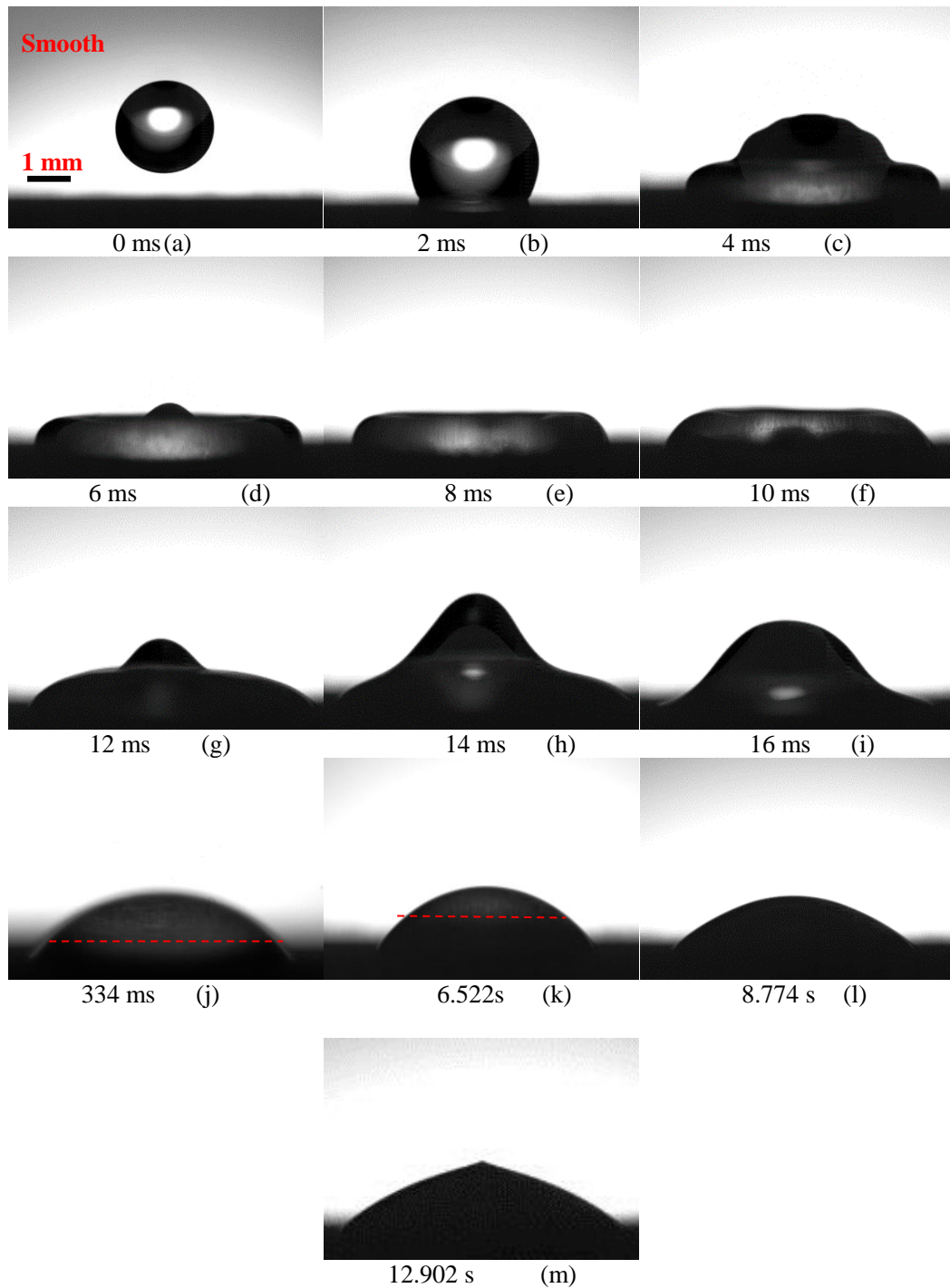


Figure 23: Images of water droplet impact on flat smooth surface ($D=2.82$ mm, $T_s=-10^\circ\text{C}$, $u=0.77$ m/s, $T_d=5^\circ\text{C}$ and $\theta=77^\circ$)

The impact process of a water droplet ($D = 2.82$ mm) on the coated varied channel textured surface at the temperature of -10°C is shown in Fig. 24. A lamella outside of the droplet formed right after the impact, and then a ring was formed. A large portion of the droplet mass stays in the outer ring instead of the inner lamella (Fig. 24 d). The first spreading process lasted about 6 ms, and the maximum spreading

diameter was 4.28 mm (Fig. 24 b-d). The retraction process started at 8 ms (Fig. 24 e). Since the coated varied channel textured surface is hydrophobic, the maximum height of the droplet can reach is larger than smooth surface during the retraction process (Fig. 24 e-h). The spreading and retracting processes can be modelled as a harmonic oscillation, and the droplet tends to spread because of the initial kinetic energy. During the spreading phase, the initial kinetic energy of the droplet was transferred to surface energy, internal energy, and kinetic energy inside the droplet. The spreading process is determined by the surface tension, viscous force, friction, and air drag [2]. Since the heat transfer rate is lower on the hydrophobic surface than hydrophilic surface due to the lower liquid-solid contact area, the viscous force of the droplet is lower on the hydrophobic surface. The viscous dissipation loss is much lower on the hydrophobic surface due to the viscous property of the liquid droplet. The dynamic phase lasted about 532 ms, and then the icing process initiated and lasted for about 21.32 s (Fig. 24 i-m). The droplet freezing process initiated at the liquid-solid interface (Fig. 24 i), and it propagated to the top of the droplet (Fig. 24 j-l). A small tip was formed on the top of the droplet at the end of the icing phase (Fig. 24 m). This pointy tip is formed when the droplet is completely frozen because the water droplet expands during freezing process. The formation of the tip can be explained by the combination of water expansion and surface tension on a spherical cap of remaining liquid [30]. Compared with the total icing time on the smooth surface, the total icing time on coated varied channel surface is much longer under the same conditions.

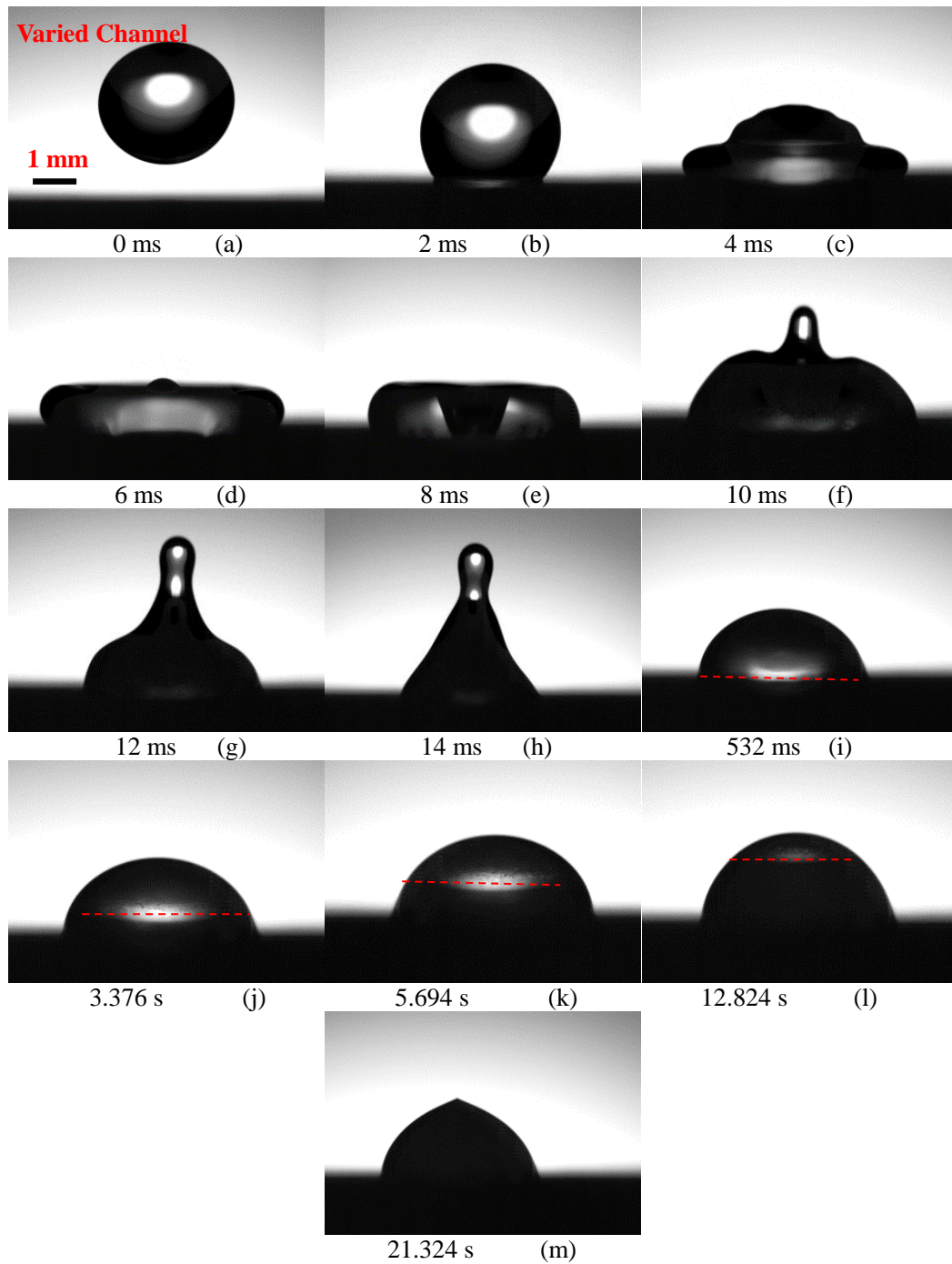


Figure 24: Images of water droplet impact on flat coated varied channel surface ($D=2.82$ mm, $T_s=-10^\circ\text{C}$, $u=0.77$ m/s, $T_d=5^\circ\text{C}$ and $\theta=145^\circ$)

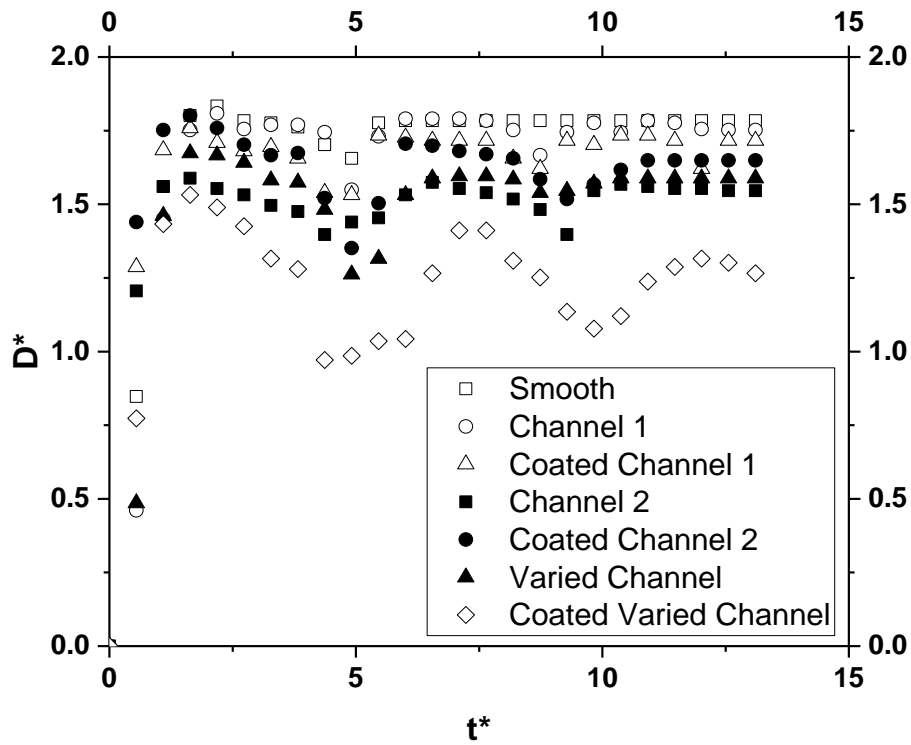


Figure 25: Droplet diameter at liquid-solid interface vs. time ($D = 2.82 \text{ mm}$, $u = 0.77 \text{ m/s}$, and $\theta = -10^\circ\text{C}$)

Two sets of droplet impact images for smooth and coated varied channel surfaces at certain conditions are shown in Fig. 23 and 24. Fig. 25 shows the variation of droplet diameters at the liquid-solid interface with respect to time for all seven different surfaces during the droplet dynamics. The $D = 2.82 \text{ mm}$ and $u = 0.77 \text{ m/s}$ and sample surface temperature is -10°C . The x-axis and y-axis represent dimensionless time and diameter which refer to Eq. 18 and 20. The data demonstrate that the droplet spreads larger on a hydrophilic surface than on a hydrophobic surface which means the maximum spreading radius decreases with lower surface wettability. The coated varied channel surface (with highest contact angle, see Table 1) shows the smallest spreading diameter. The more hydrophobic surfaces also show higher magnitude of oscillations during the dynamic processes, and much longer time is needed for a droplet to reach steady state on a hydrophobic surface than on a hydrophilic surface. The liquid-solid

interfacial tension prevents the spreading of the droplet, and this interfacial tension is higher on hydrophobic surface. The water droplet consumes less energy during the overall dynamic phase on the hydrophobic surface because of the low surface energy on the hydrophobic surface. The water droplet oscillates longer on the hydrophobic surface because of the low energy consumption during droplet dynamics. The water droplet oscillates longer and spreads less on the hydrophobic surface due to the lower surface wettability.

The Fig. 26 and 27 shows the change of droplet contact diameter at the solid-liquid interface with respect to time when $u = 0.77$ m/s and sample surface temperature = -10°C for two different droplet diameters. As seen from the figures, the droplet with 4.11 mm diameter oscillates around 40 ms and the 2.82 mm diameter droplet oscillates around 20 ms. The maximum spreading radius for 4.11 mm droplet is around 9 mm, and the maximum spreading radius for 2.82 mm droplet is around 5 mm. The water droplet spreads larger and oscillates longer for the larger water droplet because the larger droplet contains more kinetic energy.

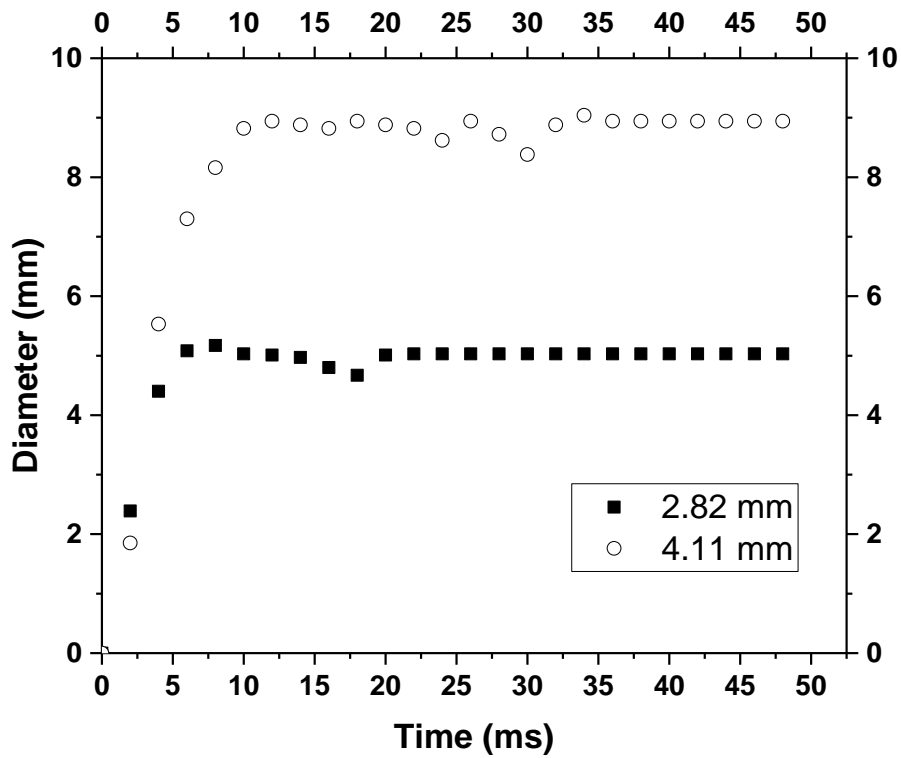


Figure 26: Droplet diameter at liquid-solid interface vs. time on smooth surface ($u=0.77$ m/s, and $T_s=-10^\circ\text{C}$)

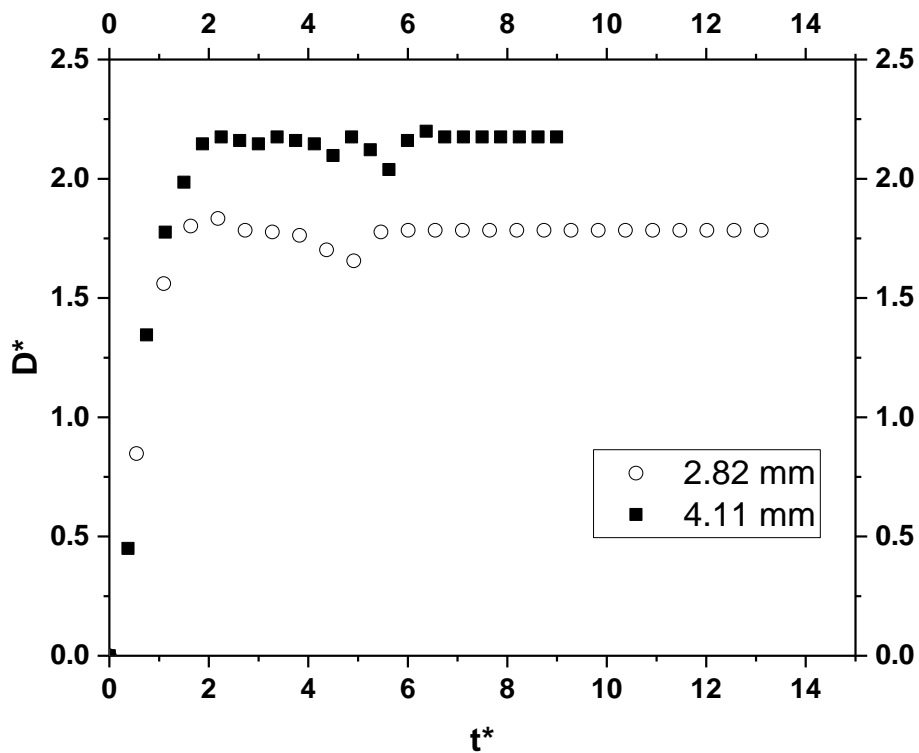


Figure 27: The change of droplet diameter with time on smooth surface ($u=0.77$ m/s, and $T_s=-10^\circ\text{C}$)

The droplet icing experiment were performed with varying parameters to find out the effects of these factors on the droplet total icing time. Both dimensional and dimensionless analysis are performed to better understand the droplet overall icing time under different conditions. Seven sample surfaces (introduced in the sample preparation section) with different wettabilities are used and five runs of experiments are conducted at each condition.

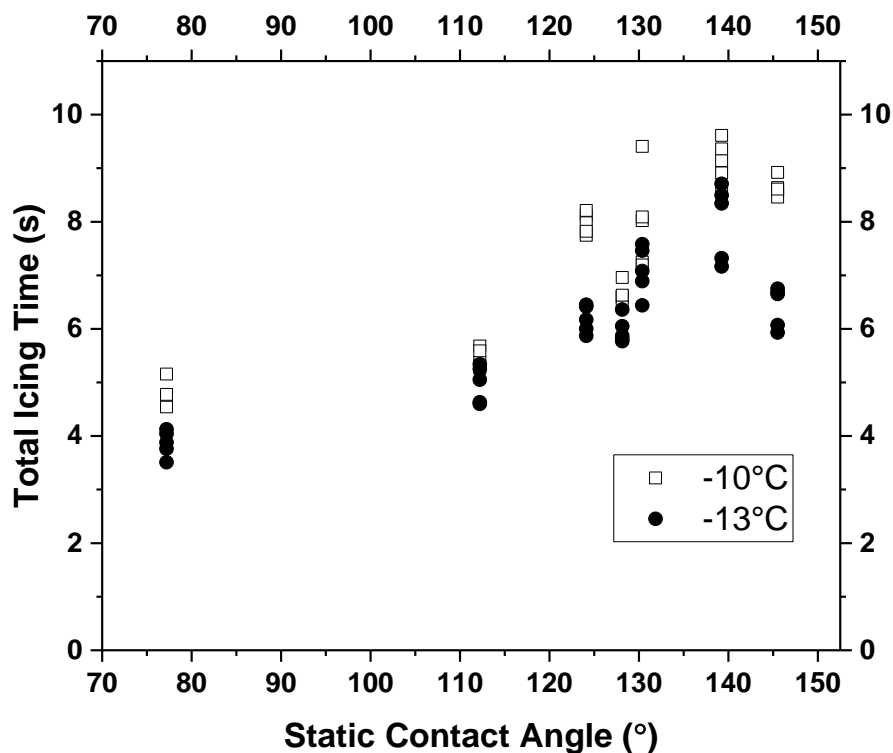


Figure 28: Droplet icing time vs. static contact angle at $u = 0.77$ m/s when $T_s = -10$ °C and -13 °C

Fig. 28 clearly demonstrates how the droplet total icing time varies with static contact angles and the surface temperatures. As the static contact angle increases (lower surface wettabilities), the total icing time increases. The droplet total icing time also increases with higher surface temperatures. Since the water droplets spread less and oscillate longer on the hydrophobic surfaces with lower wettability, the solid-liquid contact area is smaller than that on the hydrophilic surface. Smaller solid-liquid contact area leads to less amount of heat transfer, resulting in longer total

icing time on surfaces that are more hydrophobic. With lower surface temperature, the heat transfer rate increases, leading to shorter total icing time.

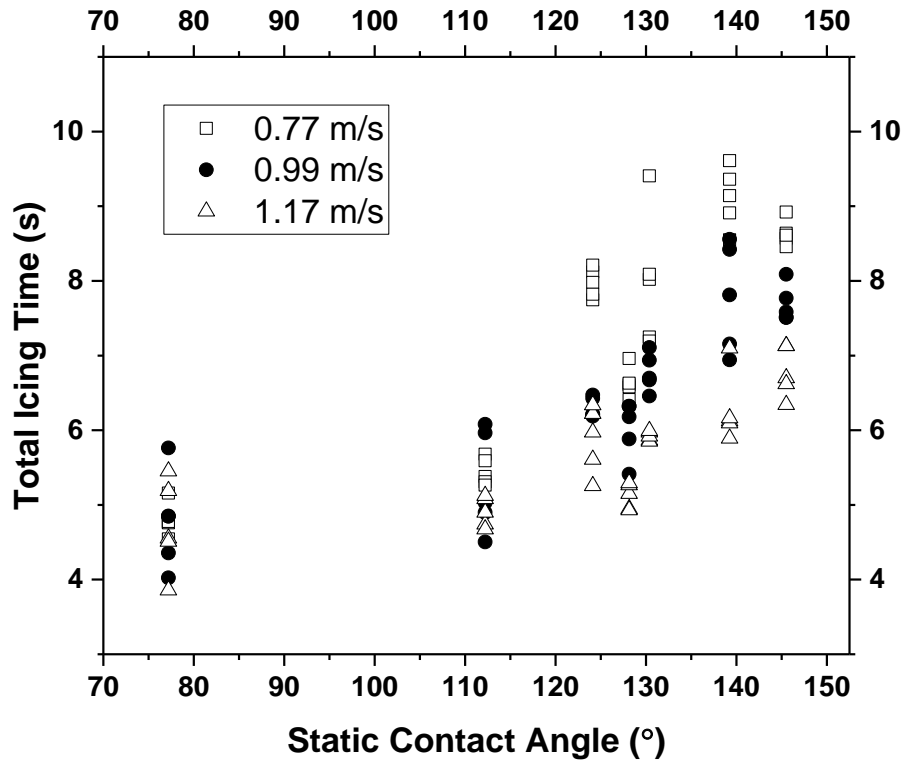


Figure 29: Droplet icing time vs. Static contact angle at $-10\text{ }^{\circ}\text{C}$ when the impact speed is 0.77 m/s , 0.99 m/s , and 1.17 m/s

Fig. 29 shows how the water droplet total icing time changes with static contact angles at different impact velocities of 0.77 m/s , 0.99 m/s , and 1.17 m/s . As seen from the figure, the total icing time decreases as the impact velocity increases. With higher impact velocity, more initial kinetic energy is available for the dynamic process, the droplet spreads faster, and the maximum contact area increases. Since the contact area and time during dynamic phase increase with the higher impact velocity, the heat transfer rate from the drop to the sample surface increases. At very high impact velocity, liquid from the droplet may also penetrate into the micro-grooves of the textured hydrophobic surfaces, leading to larger heat transfer area and higher heat transfer rate.

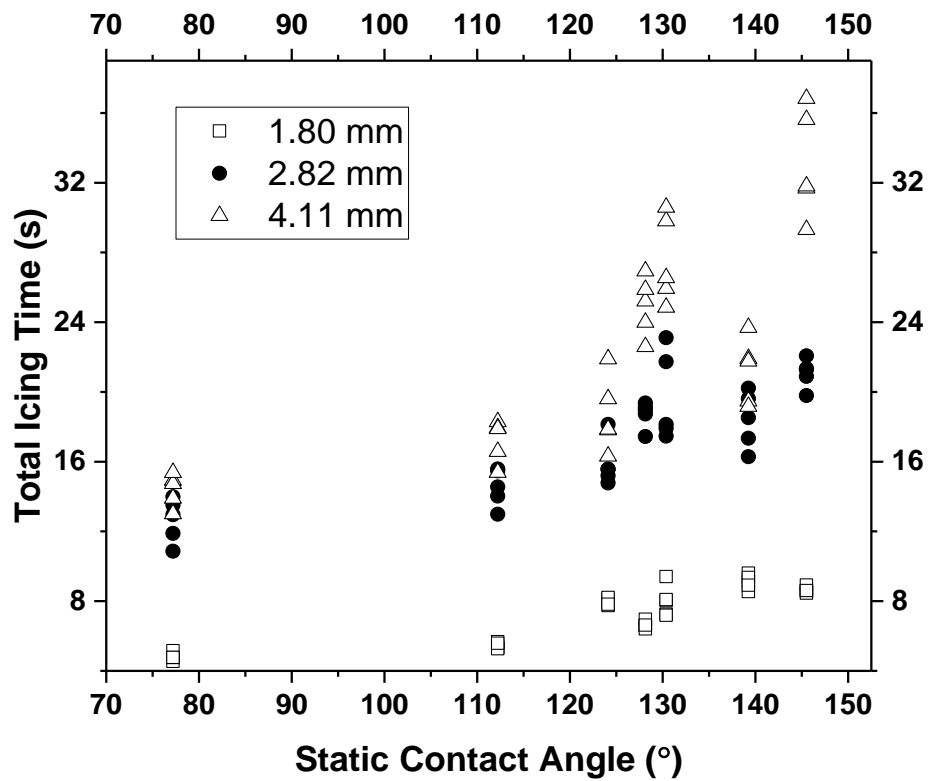


Figure 30: Droplet icing time vs. Static contact angle at -10°C when the droplet diameter is 1.8 mm, 2.82 mm, and 4.11 mm

Fig. 30 shows the relationship between the total icing time and the initial droplet diameter. As expected, larger droplets need longer total icing time. The results also demonstrate that the contribution of droplet volume (larger drops need longer icing time) is more significant than the effects of droplet spreading diameter and oscillation time (more contact area and time cause shorter icing time) since the droplet dynamic process is much shorter compared with the total heat transfer process.

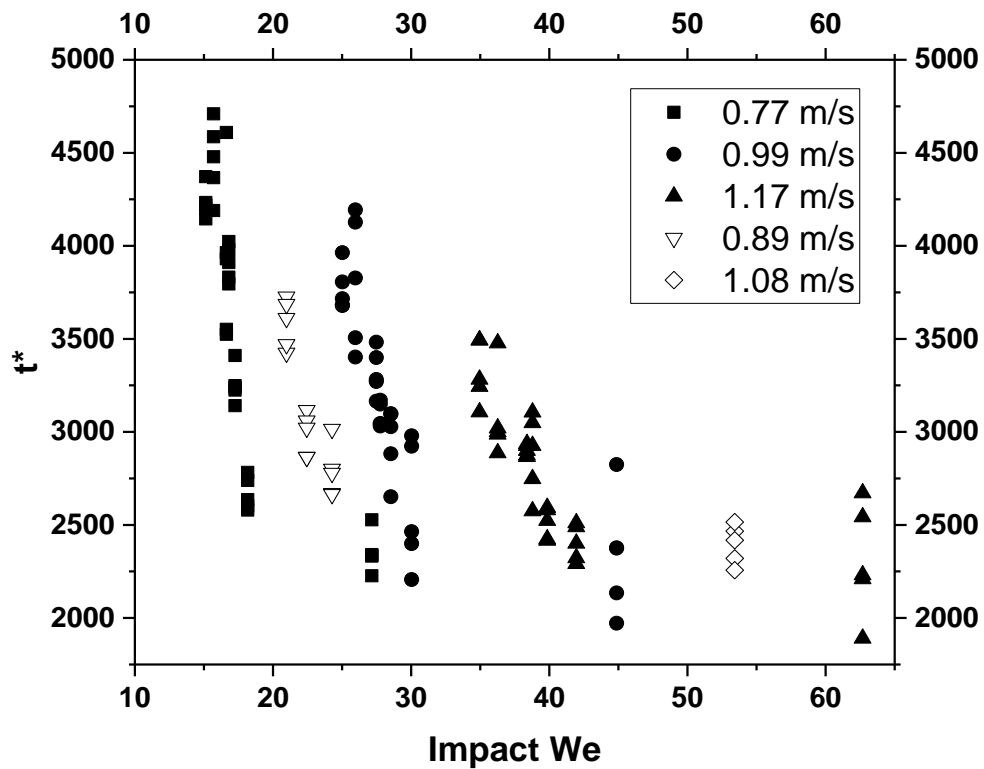


Figure 31: Dimensionless time vs. impact We at different impact velocities at -10°C

Fig. 31 and 32 show the relationship between dimensionless icing time and impact Weber number at different impact velocities and surface temperatures. The dimensionless icing time and impact Weber number can be referred to Eq. 18 and 17. The data demonstrate that the dimensionless icing time decreases with higher impact Weber numbers or lower surface temperatures. Eq. 17 shows that the impact Weber number increases as the Weber number and advancing contact angles increase. The higher impact velocity and wettability leads to shorter icing time. The Fig. 31 combines all data points under different velocities, and it also clearly shows that dimensionless time decreases while increasing impact Weber number.

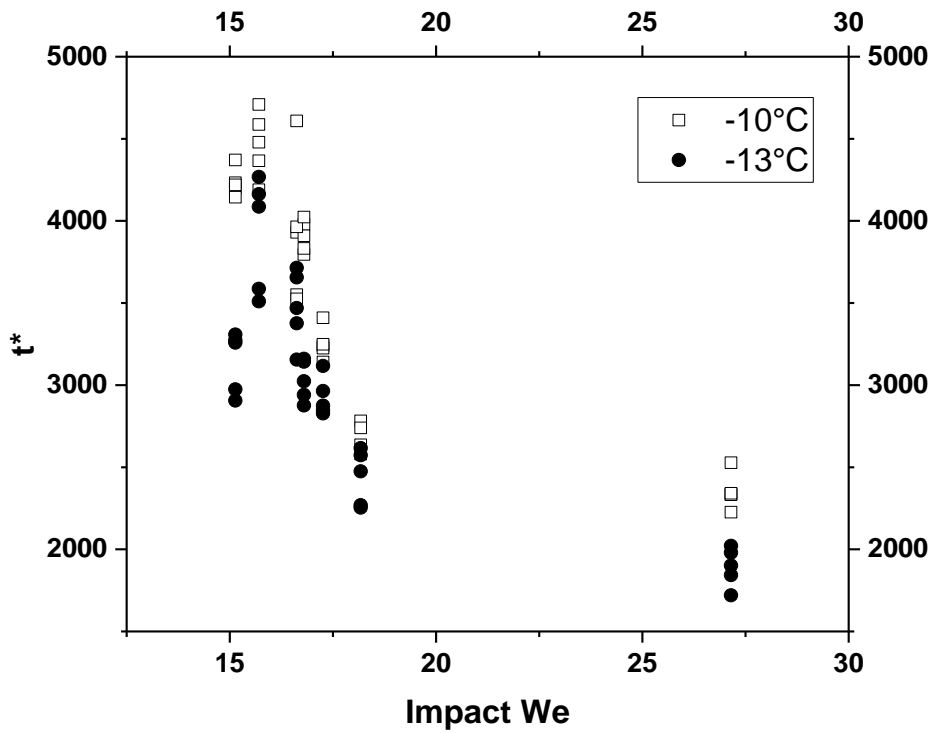


Figure 32: Dimensionless time vs. Impact We when the surface temperature is -10°C and -13°C .

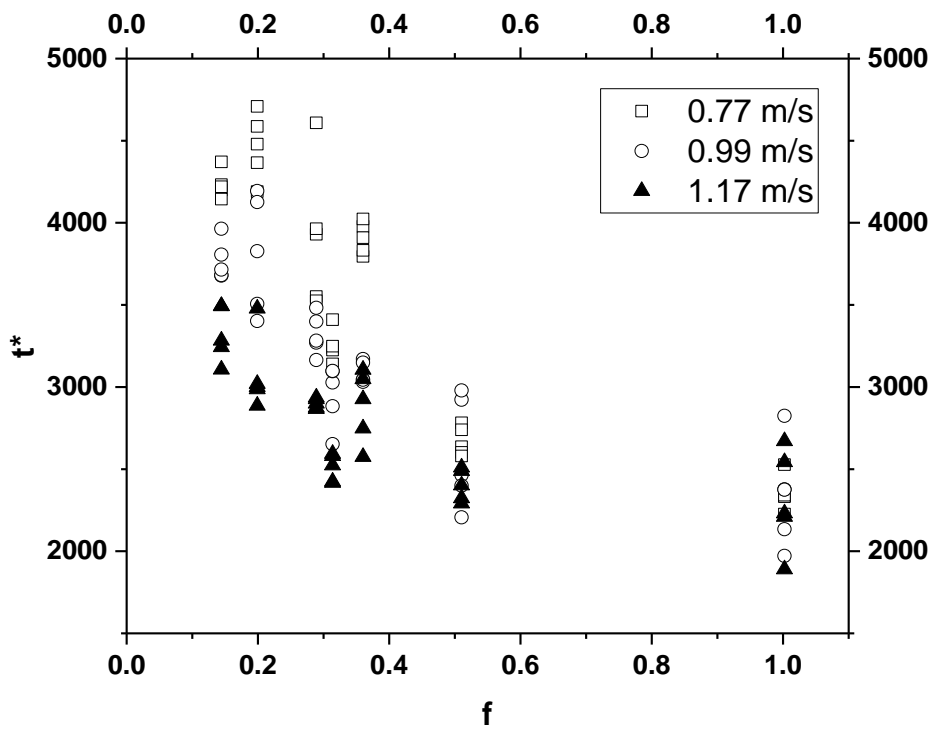


Figure 33: Dimensionless time vs. f number at different impact velocities

In Fig. 33, shows that the dimensionless total icing time decreases as the f number increases. The f number is the fraction of the solid-liquid actual contact area over the total solid surface area which is determined by Eq. 19. The contact area increases with higher f number, leading to higher heat transfer rate and lower total icing time. Lower surface wettability with low f number causes the droplet oscillates longer and spreads less during the overall dynamic phase, causing lower overall heat transfer rate on the more hydrophobic surfaces.

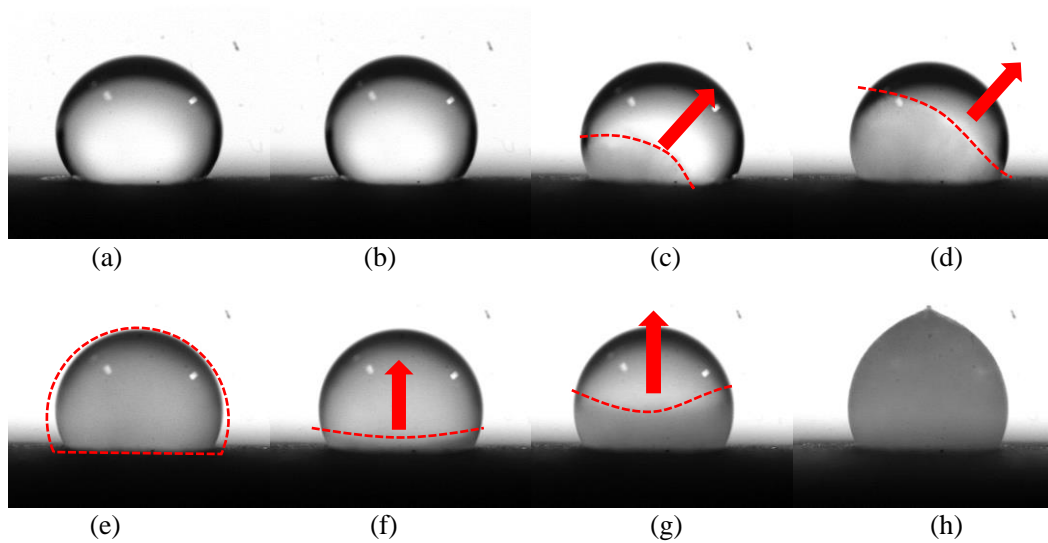


Figure 34: The detailed water droplet icing process

Fig. 34 shows a typical water droplet icing process on a hydrophobic horizontal surface. It is essential that the solid surface is wetted by the water droplet to initiate the icing process. It initiates at the solid-liquid interface (heterogeneous nucleation). Then, the ice formation propagates from the bottom to the top of the drop through the liquid-gas interface (Fig. 34 c-e). After the outer surface layer of the droplet is fully frozen, the inner portion of the droplet starts to freeze from the bottom and propagates to the top (Fig. 34 f-h). As discussed earlier, a sharp tip forms on the top of the water droplet when it is fully frozen (Fig. 34 h).

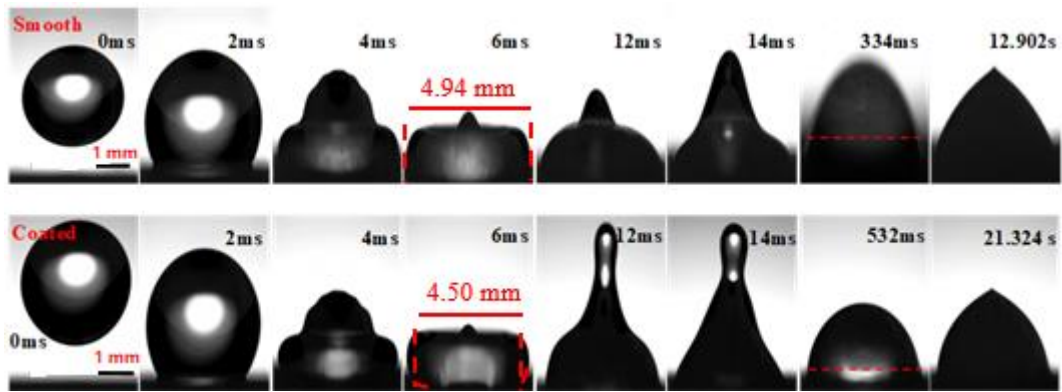


Figure 35: Water droplet impact and icing comparison on Smooth and coated varied channel surface ($D=2.82\text{ mm}$, $T_s=-10^\circ\text{C}$, $u=0.77\text{ m/s}$ and $T_a=5^\circ\text{C}$)

Fig. 35 shows the comparison of a single water droplet impact dynamics and icing on a smooth surface (hydrophilic) and a coated varied channel surface (hydrophobic). After impacting the sample surfaces, both droplets go through the spreading and retraction phases. The droplets reach the maximum spreading radius around 6 ms on both hydrophilic and hydrophobic surfaces. Between 12 ms and 14 ms, both droplets retract and lift to the maximum vertical distances. As seen from Fig. 35, there is an obvious difference in the retraction phase of the impacting droplet on the hydrophilic and the hydrophobic surface. The observation shows that the maximum height the droplet can reach is larger on the hydrophobic surface than smooth surface during the retraction process. The droplet oscillations end and the icing process starts around 334 ms on the smooth surface and 532 ms on the hydrophobic surface. There is also an obvious difference on the droplet total icing time, much longer on the hydrophobic surface than the hydrophilic surface.

4.3 Droplet Impact and Ice Formation Process on inclined Surfaces

Similar experiments were conducted to investigate droplet dynamics and icing process on inclined surfaces, which were found to be different than those on the horizontal surfaces. In the experiments, the temperature, relative humidity, and air

pressure in the laboratory were kept constant. The droplet dynamics and icing processes were captured with the high-speed camera. The temperature of the sample surface was -10°C . The droplet diameter was 2.82 mm. The droplet impact speed was 0.77 m/s. The droplet initial temperature was 5°C . The 7 sample surfaces with different wettabilities, discussed earlier, were used in these experiments.

A new coordinate system, shown in Fig. 36, was used to describe the droplet geometry during the dynamic processes. The x-axis is parallel to the sample surface and y-axis is perpendicular to the sample surface, and the origin sits in the middle of the droplet (which is now moving with the droplet). Fig. 36 shows the coordinate system of the droplet impact on the inclined surface. Fig. 37 clearly indicates the typical droplet impact and icing process on a 30° inclined smooth surface. Kinetic energy, surface tension, air drag, liquid viscosity, gravity and surface wettability play important roles during droplet impact dynamics process. The surface temperature, droplet size, and surface wettability play important roles during droplet icing process. The water droplet moves into dynamic phase after impacting the sample surface, and the ice nucleation phase (phase change) occurs after the dynamic phase. The dynamic phase contains spreading phase (Fig. 37 b-e), gliding phase (Fig. 37 f-g), and relaxation phase (Fig. 37 h-j). The dynamic phase lasted 255 ms before moving into icing phase. The impact process of a water droplet ($D = 2.82$ mm) on the smooth sample surface at the temperature of -10°C and impact speed at 0.77 m/s is shown in Fig. 37. The moment when the droplet first impacted the sample surface was defined as the starting point. After hitting the sample surface, a lamella was formed from the base of the water droplet, and then a ring was formed which means the most volume of droplet stayed in the outside ring instead of inside lamella (Fig. 37 b-e). At the end of the spreading phase, the water droplet reached to its maximum spreading contact diameter (Fig. 37 e).

During the spreading phase, the kinetic energy of the impinging water droplet was transferred to surface energy, internal energy, and kinetic energy inside the droplet. The total spreading process lasted for 5 ms on a smooth surface. The gliding phase started right after the spreading phase (Fig. 37 f-g). During the gliding phase, the water droplet started to slide downward along the surface due to gravity. Since the foremost point of the droplet moved faster than the rearmost point of the droplet, the water droplet elongated further. Then, the relaxation phase which contained number cycles of droplet forward and backward movements (Fig. 37 g-i). The droplet becomes steady and reached its equilibrium state of about 255 ms. The ice formation phase started after the dynamic phase, and the water droplet took about 9.2325 s to freeze. The droplet freezing process initiated at the liquid-solid interface (Fig. 37 j), and it propagated to the top of the droplet (Fig. 37 k). A small tip was formed on the top of the droplet at the end of the icing phase (Fig. 37 l).

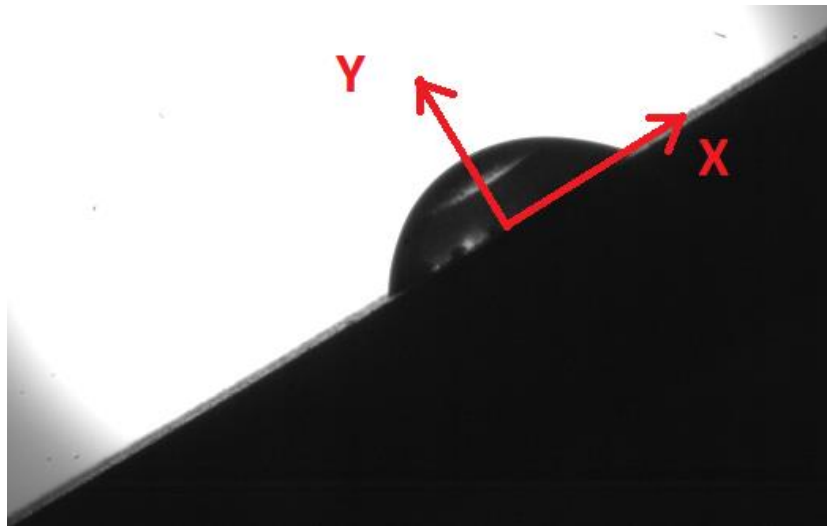


Figure 36: Coordinate system of droplet impact movement on inclined surface

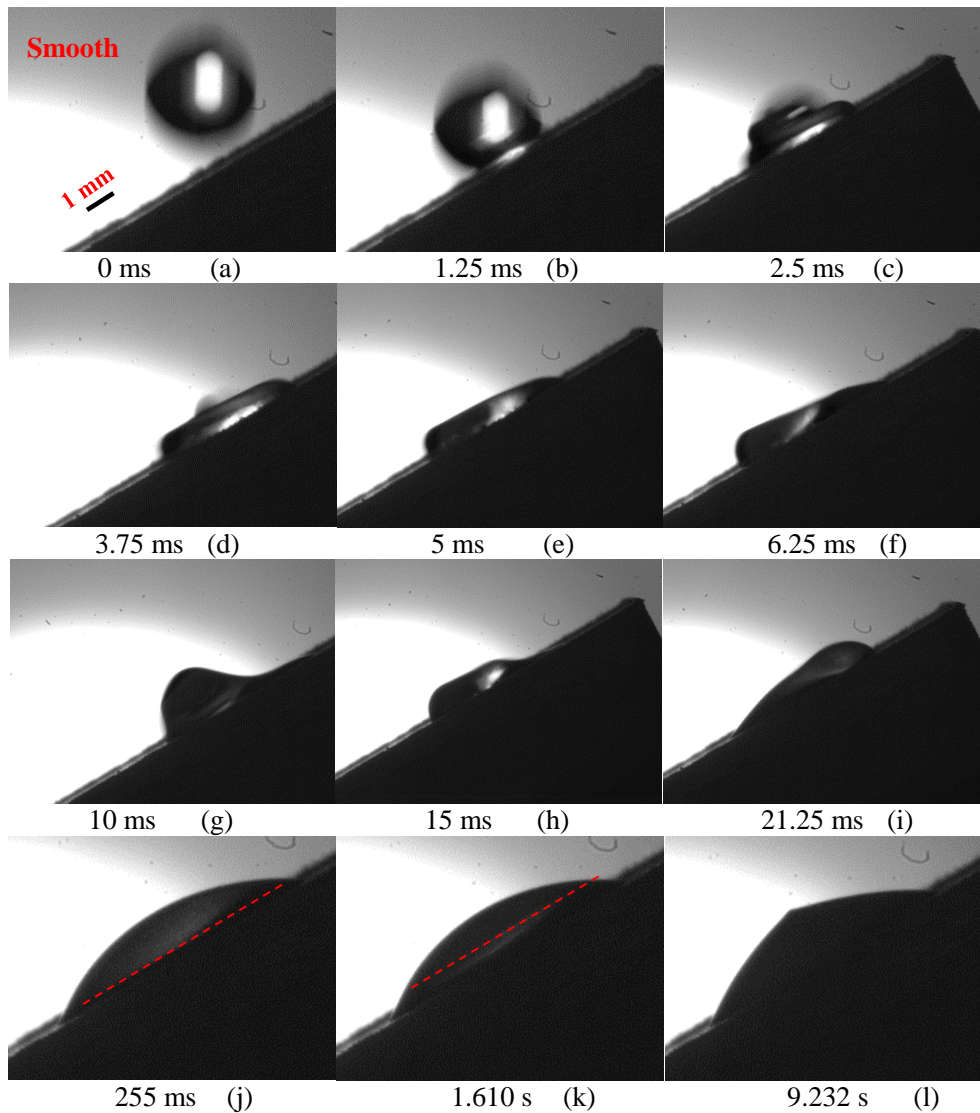
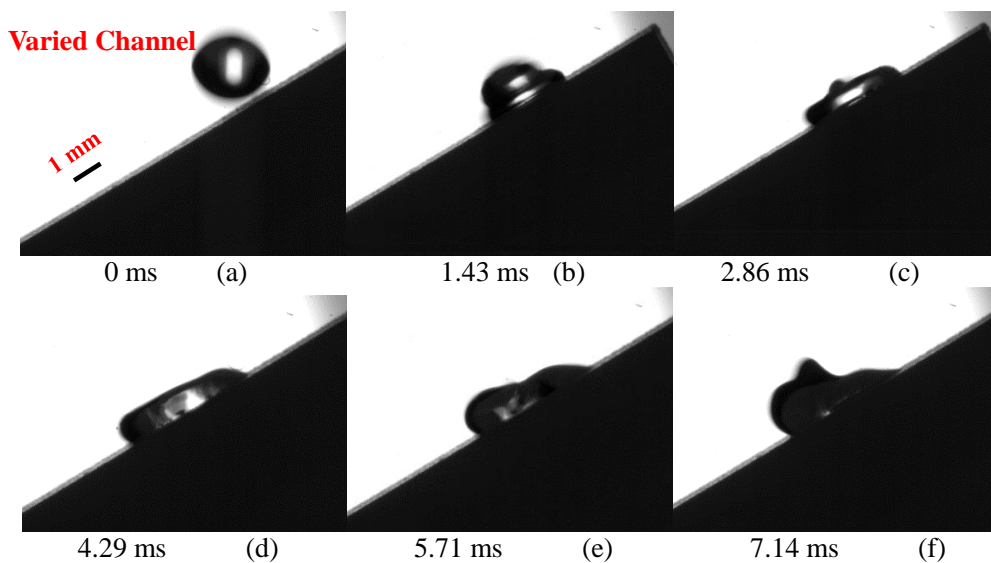


Figure 37: Images of water droplet impact on the smooth surface with the inclined angle of 30° ($D=2.82$ mm, $T_s=-10^\circ\text{C}$, $u=0.77$ m/s, $T_d=5^\circ\text{C}$ and $\theta=77^\circ$)

Fig. 37 shows the typical droplet impact and icing process on a 30° inclined coated varied channel surface. The water droplet moves into dynamic phase after impacting the sample surface, and the ice nucleation phase (phase change) occurs after the dynamic phase. The dynamic phase contains the spreading phase (Fig. 37 b-d), the gliding phase (Fig. 37 e-g), and the relaxation phase (Fig. 37 h-k). The dynamic phase lasted 344.29 ms before moving into icing phase. The impact process of a water droplet ($D= 2.82$ mm) on the coated varied channel surface at the temperature of -10°C and impact speed at 0.77 m/s is shown in Fig. 37. After hitting

the sample surface, a lamella was formed from the base of the water droplet, and then a ring was formed. The most volume of droplet stayed in the outer ring instead of the inner lamella (Fig. 37 b-d). At the end of the spreading phase, the water droplet reached to its maximum spreading contact diameter (Fig. 37 d). During the spreading phase, the kinetic energy of the impinging water droplet was transferred to surface energy, internal energy, and kinetic energy inside the droplet. During the gliding phase, the water droplet started to slide downward along the surface due to gravity. Since the foremost point of the droplet moved faster than the rearmost point of the droplet, the water droplet elongated further. Then comes the relaxation phase, which contained a number of cycles of droplet movements forward and backward (Fig. 37 g-j). It took about 13.68 s for the water droplet to completely freeze. The droplet freezing process initiated at the liquid-solid interface (Fig. 37 k), and it propagated to the top of the droplet (Fig. 37 l-m). A small tip was also formed on the top of the droplet at the end of the icing phase (Fig. 37 n). Compared with droplets on the smooth (hydrophilic) surface, the total icing time on coated varied channel surface was much longer, which can be explained by the same reasons as explained for drops on the horizontal surface.



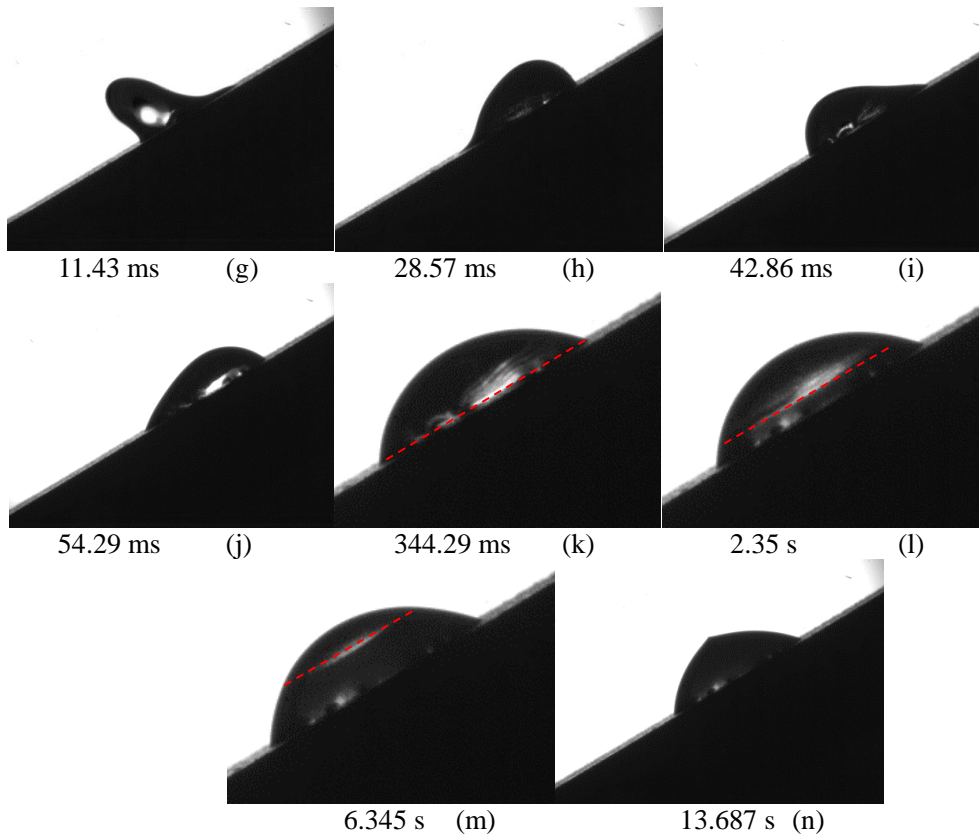


Figure 38: Images of water droplet impact on coated varied channel surface with an inclined angle of 30° ($D=2.82$ mm, $T_s=-10^\circ\text{C}$, $u=0.77$ m/s, $T_d=5^\circ\text{C}$ and $\theta=145^\circ$)

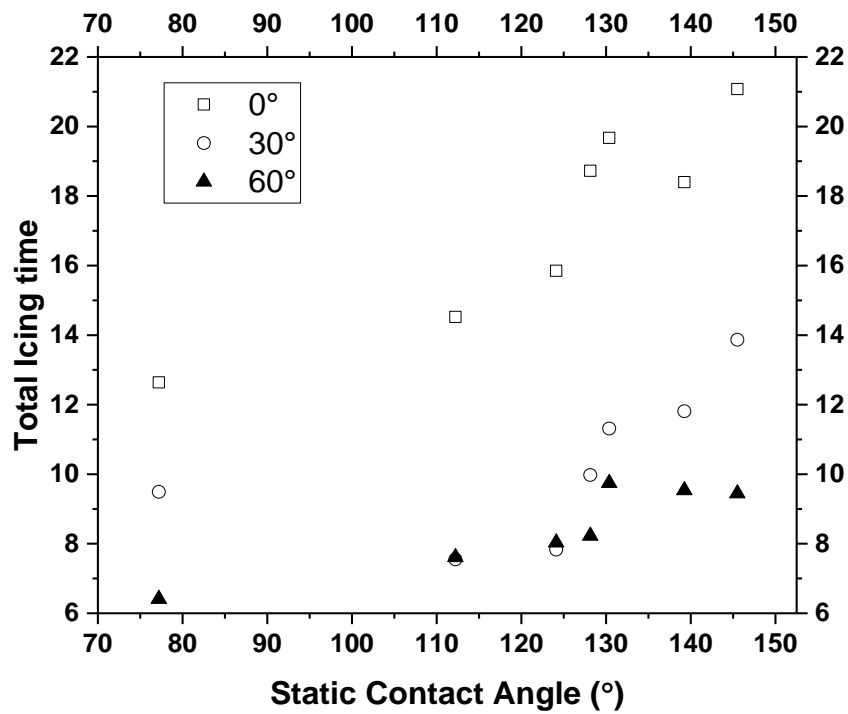
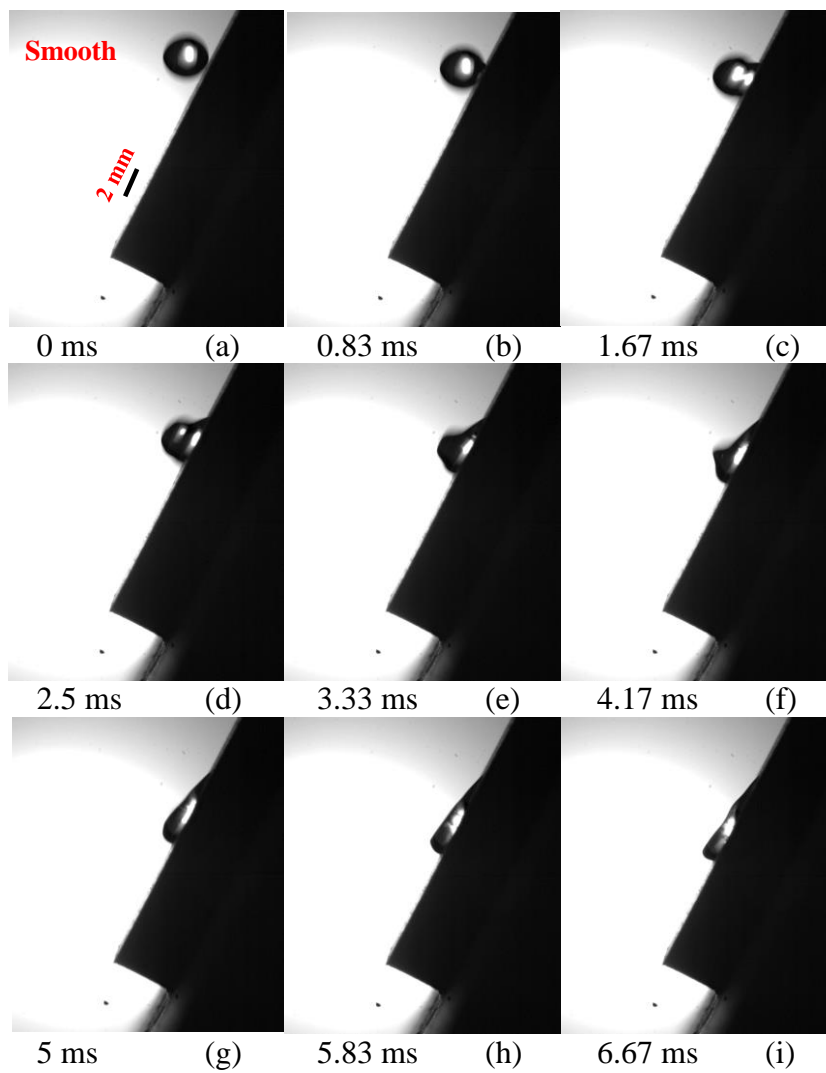


Figure 39: Total icing time vs. Static contact angle at three different inclined angles which are flat, 30° , and 60° . ($D=2.82$ mm, $T_s=-10^\circ\text{C}$, $u=0.77$ m/s, and $T_d=5^\circ\text{C}$)

Fig. 39 shows how the total icing time changes with surface wettability and inclined angles. The total icing time increases as the wettability decreases on both horizontal and inclined surfaces. The data suggest that the total icing time is shorter on inclined surfaces since the solid-liquid contact area increases due to the droplet gliding process, leading to higher heat transfer rates. The droplet total icing time decreases as the inclined angle increases. Since the droplet glides longer distance due to gravity and the inclined angle, the liquid-solid contact area increases during the gliding process.



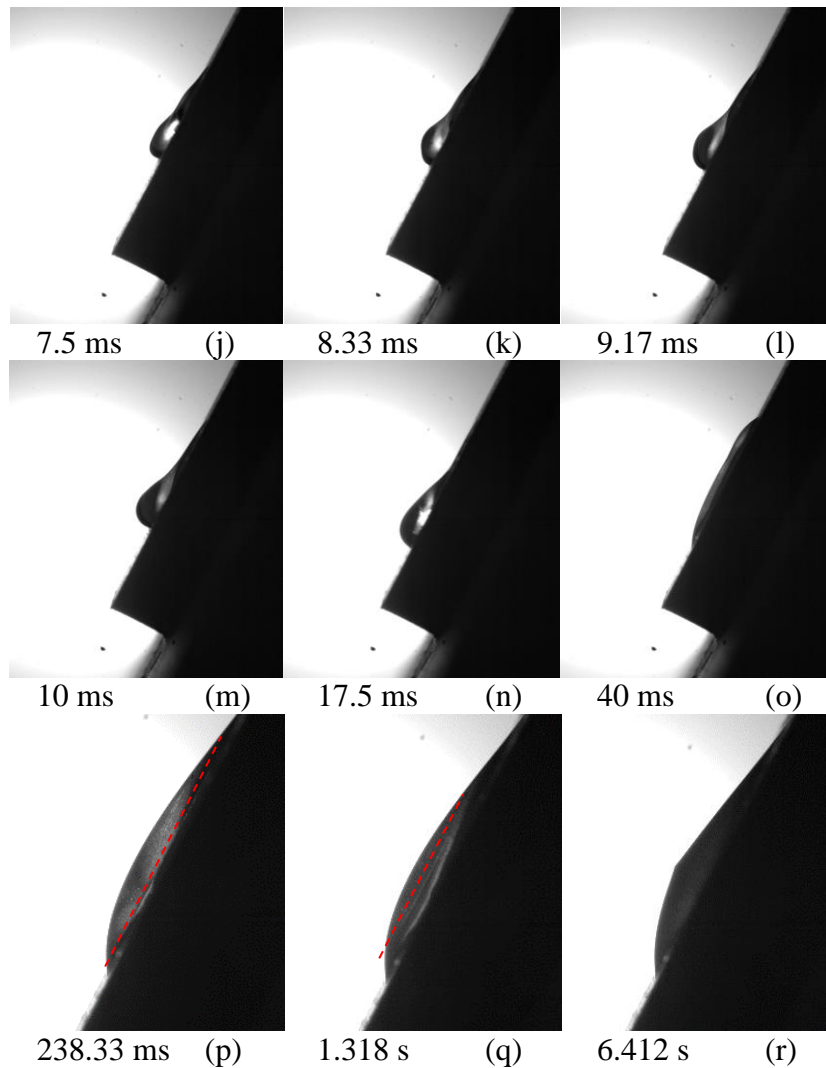
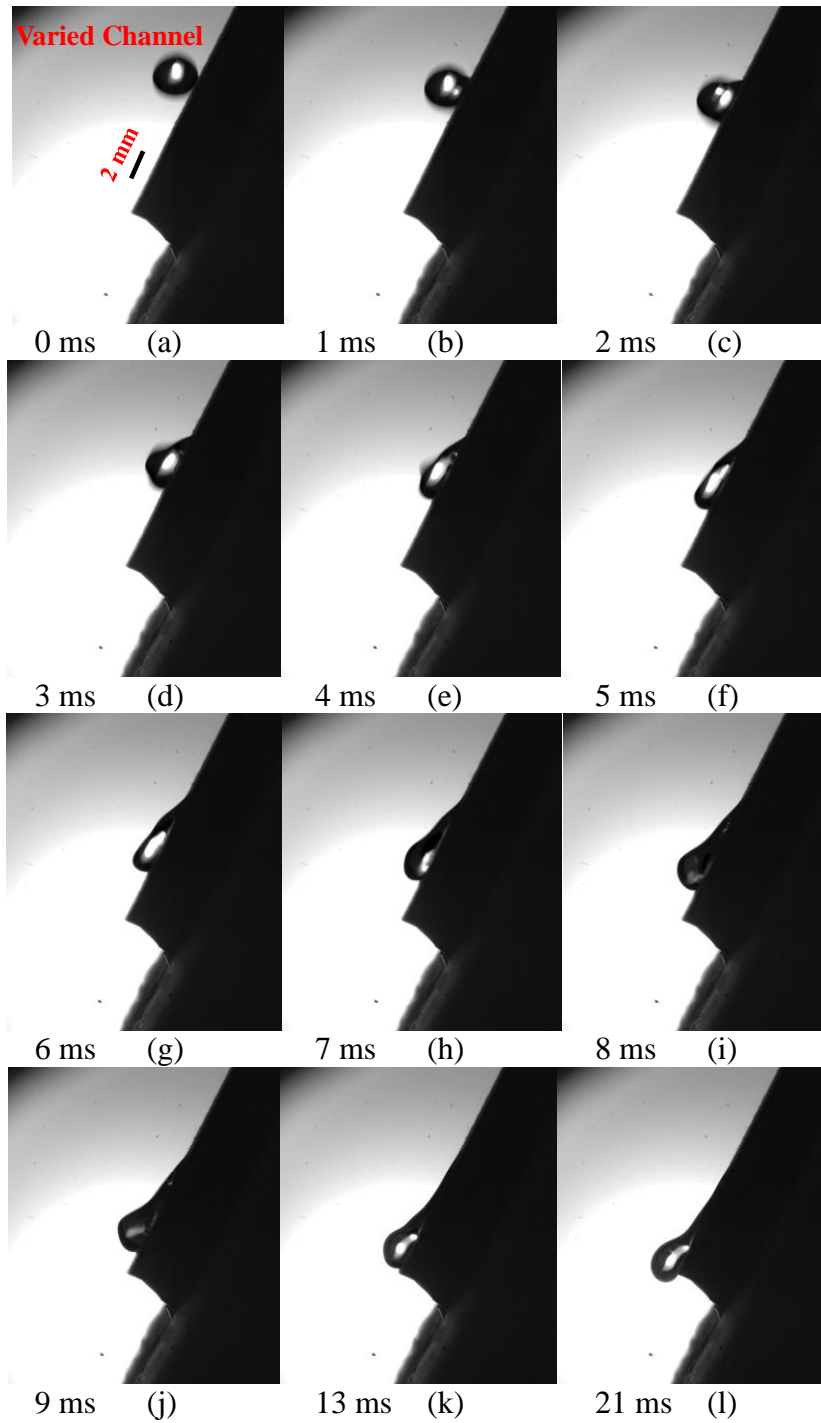


Figure 40: Images of water droplet impact on the smooth surface with an inclined angle of 60° ($D=2.82$ mm, $T_s=-10^\circ\text{C}$, $u=0.77$ m/s, $T_d=5^\circ\text{C}$ and $\theta=77^\circ$)

Fig. 40 clearly indicates the typical droplet impact and icing process on a 60° inclined smooth surface. The water droplet goes to dynamic phase after impacting the sample surface, and the ice nucleation phase (phase change) occurs after the dynamic phase. The dynamic phase contains spreading phase (Fig. 40 b-h), gliding phase (Fig. 40 i-n), and relaxation phase. The dynamic phase lasted 238 ms before moving into ice formation process. The total spreading process lasted for 5.83 ms on the smooth surface. The droplet becomes steady and reached its equilibrium state of about 238 ms. The droplet icing phase started after the dynamic phase, and the water droplet took about 6.412 s to freeze. The droplet freezing process initiated at the liquid-solid

interface (Fig. 40 p), and it propagated to the top of the droplet (Fig. 40 q). A small tip was formed on the top of the droplet at the end of the ice formation phase (Fig. 40 r).



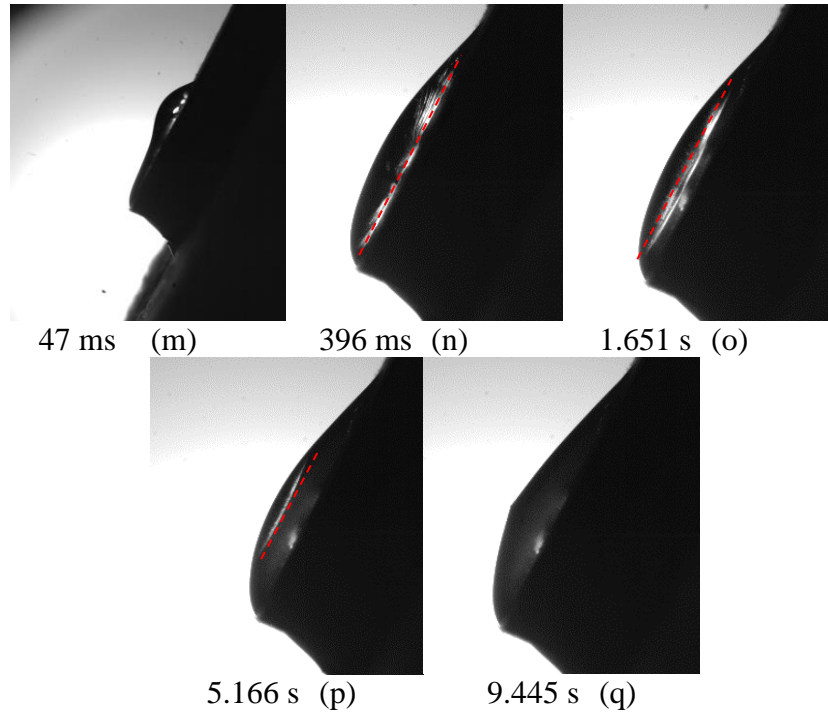
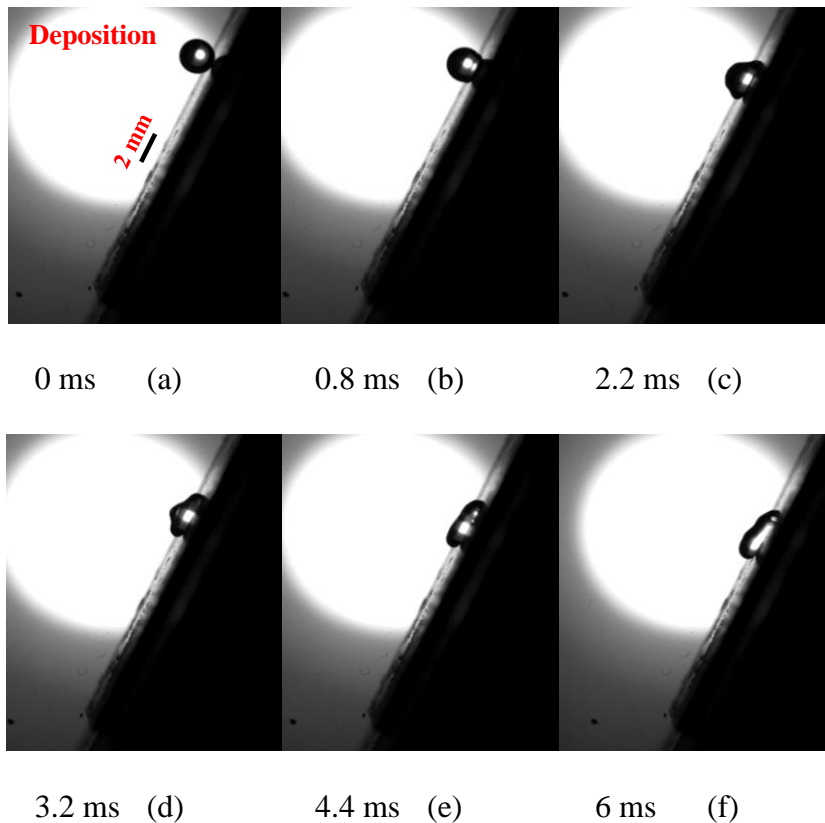


Figure 41: Images of water droplet impact on coated varied channel surface with inclined angle of 60° ($D=2.82$ mm, $T_s=-10^\circ\text{C}$, $u=0.77$ m/s, $T_a=5^\circ\text{C}$ and $\theta=145^\circ$)

The impact process of a water droplet ($D=2.82$ mm) on the coated varied channel textured surface at the temperature of -10°C and 60° inclined angle is shown in Fig. 41. The first spreading process lasted about 6 ms (Fig. 41 b-g). The gliding phase started right after spreading phase (Fig. 41 h). Since coated varied channel textured surface is hydrophobic surface and inclined angle increases to 60° , the height of the droplet and rolling distance can reach is larger than smooth surface during gliding process (Fig. 41 h-l). The dynamic phase lasted about 396 ms, and then the ice nucleation process initiated and lasted for about 9.445 s (Fig. 41 n-q). The droplet freezing process initiated at the liquid-solid interface (Fig. 41 n), and it propagated to the top of the droplet (Fig. 41 o-p). A small tip was formed on the top of the droplet at the end of the droplet icing phase (Fig. 41 q). Compared with total icing time on the smooth surface, the total icing time on coated varied channel surface is much longer under the same conditions.

Compared with experimental results on the 30° and 60° inclined surfaces, droplet

impact and ice formation process are different due to surface wettability, gravity, and inclined angle. The droplet total icing time decreases as increasing the inclined angle. Since the droplet glides more distance due to gravity and inclined angle effects, the real liquid-solid contact area increases during gliding process. The droplet total icing time decreases due to gliding process. The inclined angle has little effect on the total time consumed in dynamic process on both smooth and coated varied channel surfaces. As increasing the inclined angle of the surface to 60° , the droplet glides more distance and rolls off to the bottom edge of the coated varied channel surface due to gravity and surface wettability effects (Fig. 41 1). The droplet rolls back from the bottom edge of the surface to the top during relaxation process due to the surface tension of the droplet, solid surface wettability and droplet internal kinetic energy.



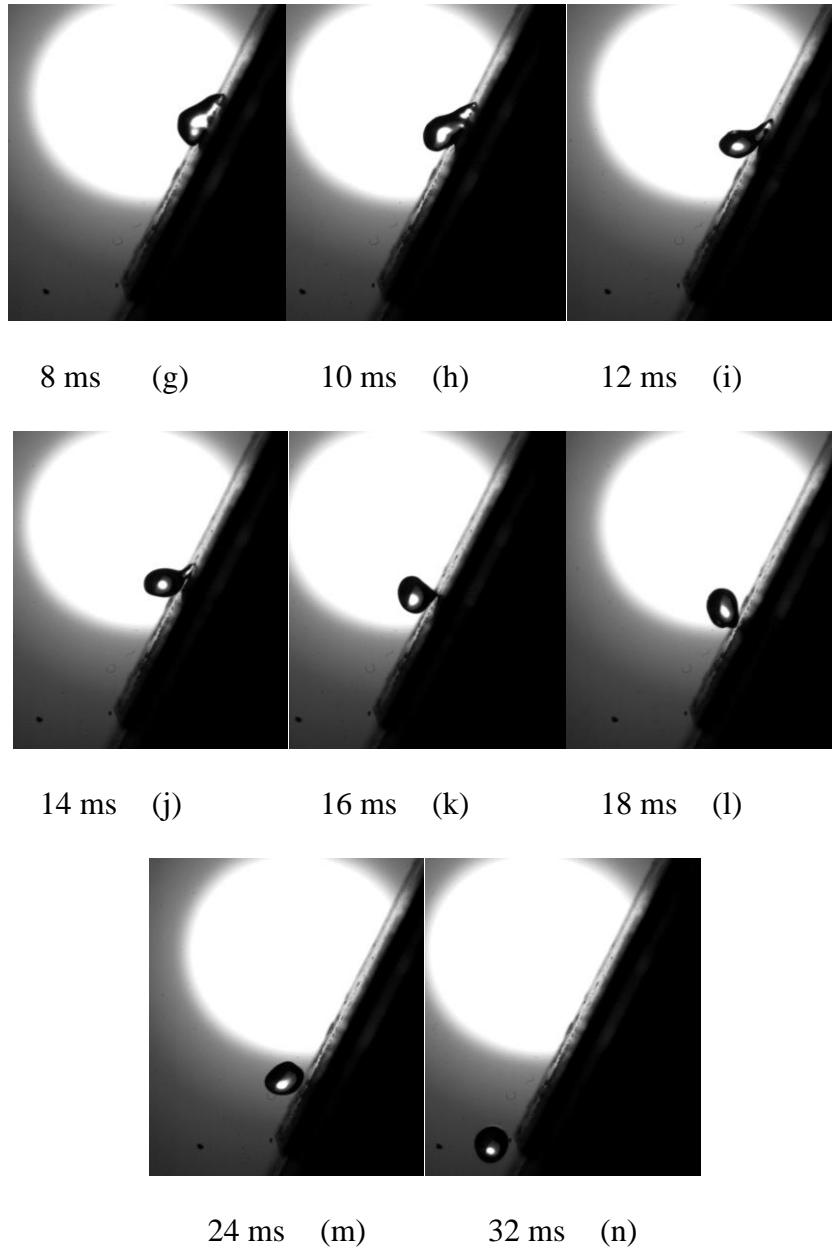


Figure 42: Images of water droplet impact on electrodeposition with an inclined angle of 60° ($D=2.82$ mm, T_s = room temperature, $u=0.77$ m/s, $T_d=5$ °C, and $\theta=145^\circ$)

The electrodeposition sample was tested with an inclined angle of 60° under room temperature. Since the sample surface is superhydrophobic and it was at room temperature, the droplet impacted on the inclined surface and bounced off (Fig. 42 k). The only spreading process lasted about 4.4 ms (Fig. 42 b-e). The gliding phase started right after spreading phase and lasted about 10 ms (Fig. 42 f-k). The receding phase was replaced by bouncing off phenomena. The droplet bounced off the superhydrophobic

surface at 18 ms (Fig. 42 1).

As seen from Fig. 43, the total icing time increases as advancing contact angle increases. A very reasonable hypothesis that the droplet total icing process is also related to the dynamic contact angle of the sample surface since the contact angle hysteresis plays an important role in the droplet dynamics. The sudden decrease of the total icing time when the advancing contact angle is from 130° to 140° may cause by experimental uncertainty. The total icing time decreases as increasing the inclined angle. The liquid-solid contact area increases as increasing inclined angle since the droplet glides further. The droplet also glides further at the same inclined angle when the advancing contact angle increases.

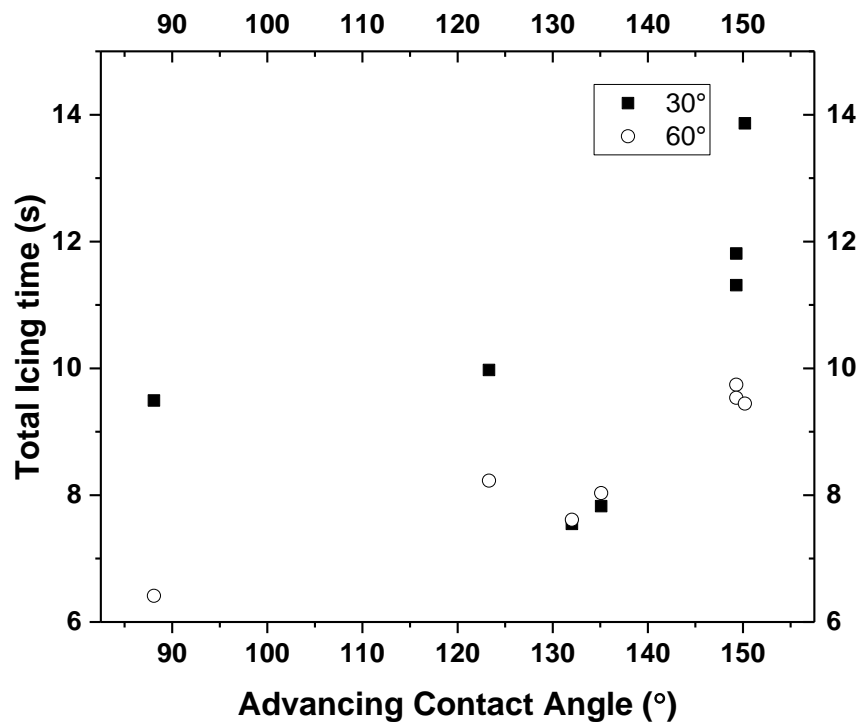


Figure 43: The effect of advancing contact angle of sample surface on droplet total icing time with inclined angles of 30° and 60°

Table 9: The wettability measurement after icing experiment

Wettability	Contact Angle (°)						
	Smooth	Channel 1	Channel 2	Coated channel 1	Varied channel	Coated channel 2	Coated varied channel
CA	85±3°	101±5°	115±5°	130±5°	134±5°	131±5°	133±4°
ACA	88±3°	105±5°	118±5°	140±5°	143±5°	137±5°	143±4°
RCA	52±3°	71±5°	77±5°	120±5°	126±5°	114±5°	109±4°
Hysteresis	35±3°	34±5°	40±5°	20±5°	16±5°	23±5°	33±4°

The wettability measurement is taken after droplet dynamics and icing experiment. The CA, ACA, RCA in table 9 represents the static contact angle, advancing contact angle, and receding contact angle. Comparing with the measurement taken before the droplet dynamics and icing experiment, the static contact angle of channel 1, channel 2, coated channel 2 and coated varied channel reduce after the experiment. The icing de-icing cycles wear the micro and hierarchical structure on the sample surface, and the cycles may also wear the Aculon coating applied on the surface. The surface wettability becomes higher after the experiment due to the changes of the surface microstructure, surface chemistry, and coating performance.

4.4 Summary

This chapter presents ANOVA and dimensional analysis of the droplet dynamics and ice formation experiments. Both flat and inclined surfaces are considered for droplet dynamics and icing process. A detailed single droplet ice formation process is also presented in this chapter. Based on experimental results and analysis, increasing droplet diameter, decreasing droplet impact speed, or increasing surface wettability can decrease the droplet total icing time. The ANOVA results agrees with the OFAT results for droplet dynamic process. The inclined angle also reduces the droplet total icing time. Chapter 5 presents conclusions and future work for my research topic.

Chapter 5

Conclusions and Recommendations for Future Work

5.1 Conclusions

This study used both statistical design of experiment and one-factor-at-a-time techniques to determine the effects of the surface temperature, impact speed, droplet temperature, surface wettability, droplet diameter, and surface inclined angle on the droplet impact dynamics and icing on different surfaces. A two-level four-factor face-centered composite design was used to investigate the effect of all four factors. Based on the DOE analysis, the surface wettability is the most important factor on the oscillation time. The droplet oscillates longer on a hydrophobic surface than the hydrophilic surface in a cold environment. The sample surface temperature and the droplet temperature have a positive effect on the oscillation time for hydrophobic surfaces, but not for a hydrophilic surface. Moreover, the impact speed has a negative impact on the oscillation time, because a larger spreading area under greater height induces a faster solidification process and viscosity reduction. A longer oscillation time increases total icing time during a freezing process; and droplet bouncing off from the surface is expected for the superhydrophobic surface.

The droplet icing experiments were performed with varying parameters including droplet impact speed, droplet diameter, sample surface temperature, and surface wettability. Based on the results and analysis, the total icing time increases with lower wettability. The icing time decreases with lower surface temperature. The actual contact area between the droplet and the hydrophobic surface is much smaller than the

hydrophilic surface since the droplet partially sits on the superhydrophobic surface. The total icing time decreases with higher droplet impact velocity since the droplet spreads more and the maximum ring radius is larger during the spreading process which results in a faster heat transfer rate. The droplet diameter and surface wettability increases, the droplet icing time increases. Since the volume of droplet increases with a larger diameter, it needs more time and overall heat transfer to fully freeze, and the contribution of a larger volume of the droplet is more significant than the droplet spreading diameter and oscillation time since the spreading process is relatively short compared with total heat transfer process. Based on experimental results and analysis, increasing droplet diameter, decreasing droplet impact speed, or increasing surface wettability can decrease the droplet total icing time.

The water droplet spreads more and oscillates longer with larger droplet diameter because the larger droplet contains more kinetic energy. Since the water droplet spreads less, oscillate longer, and partially sits on the hydrophobic surface with low wettability, the contact area at the solid-liquid interface is much smaller than the hydrophilic surface, so the ice formation initiates earlier on a smooth surface than the hydrophobic surface. The total icing time is much longer on the hydrophobic surface with low wettability due to smaller solid-liquid contact area which means lower heat transfer rate. The total icing time decreases as the impact velocity increases. The droplet may also penetrate the micro-grooves on the hydrophobic surfaces while increasing impact velocity. The droplet penetration also increases heat transfer rate between the droplet and surface. The volume of droplet increases as the diameter increases, more overall heat transfer and more time is needed to fully freeze the droplet.

5.2 Recommendations for Future Work

Several suggestions can be made for future research on this subject. Since the surface is under a very low temperature, the condensation on the sample surface damages the water repellent and de-icing performance of hydrophobic and superhydrophobic surfaces. To mitigate the condensation issue at low temperature, the experiment can be conducted in cold chamber or cold room. The high-speed droplet impact on water repellent surface experiment can be conducted in the future to better understand the relationship between the droplet impact speed and the surface wettability or total icing time. While increasing the droplet impact speed, the frames per second captured by high-speed camera should be increased to capture a clear and detailed droplet impact video. The more precise microscope connected with the high-speed camera is recommended in future droplet impact and icing experiment to capture clearer images. More water-repellent surfaces with different structures and wettabilities can be tested for the droplet dynamic and icing. Numerical simulation of the droplet dynamics and ice formation on water repellent surfaces can be conducted to compare with experimental results. The research makes a great contribution to the de-wetting and de-icing property on a metal surface in the harsh environment, for example, power transmission line, engineering construction, and pipelines. Researchers should explore different designs of surface micro-structure and further reduce surface wettability to develop icephobic metal surfaces.

References

1. Sojoudi, H., Wang, M., Boscher, N. D., Mckinley, G. H. and Gleason, K. K. “Durable and Scalable Icephobic Surfaces: Similarities and Distinctions From Superhydrophobic Surfaces”, *Soft Matter* (2016), Vol 12, pp. 1938-1963.
2. Bahadur, V., Mishchenko, L., Hatton, B., Taylor, A. J., Aizenberg, J., and Krupenkin, T., 2011. “Predictive Model for Ice Formation on Superhydrophobic Surfaces” *Langmuir*, Vol 27, pp. 14143-14150.
3. Yamada, Y., Ikuta, T., Nishiyama, T., Takahashi, K., and Takata, Y., “Droplet Nucleation on a Well-Defined Hydrophilic -Hydrophobic Surface of 10 nm Order Resolution”, *Langmuir* 2014, Vol 30, pp. 14532-14537.
4. Civil Aviation Authority. *Aircraft Icing Handbook*, 2000.
5. Volat, C. and Farzaneh, M. “De-icing/Anti-icing Techniques for Power lines: Current Methods and Future Direction.” *IWAIS XI*, Montreal, June 2015.
6. Sullivan, C.R., Petrenko, V. F., McCurdy, J. D. and Kozliouk, V. “Breaking the Ice: De-icing Power Transmission Lines with High-frequency, High-voltage Excitation”. *IEEE Industry Applications Magazine*, Vol. 9, pp. 49-54.
7. Liu, H., Gu, X. and Tang, W. “Icing and Anti-Icing of Railway Contact Wires”. *Reliability and Safety in Railway*. 2012.
8. Meuler, A. J., Smith, J. D., Varanasi, K. K., Mabry, J. M., Mckinley, G. H., and Cohen, R. E. “Relationship between Water Wettability and Ice Adhesion”. *ACS Appl. Mater. Interfaces*, 2010, 2(11), pp. 3100-3110.

9. Cao, L., Jones, A. K., Sikka, V. K., Wu, J. and Gao, D. "Anti-Icing Superhydrophobic Coatings". *Langmuir* 2009, 25(21), 12444-12448.
10. Unnikrishnan, P. K., Vaikuntanathan, V. and Sivakumar, D. "Impact Dynamics of High Weber Number Drops on Chemically Modified Metallic Surfaces". *Colloids and Surfaces A: Physicochemical and Engineering Aspects*, 459 (2014), 109-119.
11. Mandal, D. K., Criscione, A., Tropea, C. and Amirfazli, A. "Shedding of Water Drops from a Surface Under Icing Conditions". *Langmuir* (2015), 31, 9340-9347.
12. Mishchenko, L., Hatton, B., Bahadur, V., Taylor, A., Krupenkin, T., and Aizenbery, J. "Design of Ice-free Nanostructured Surfaces Based on Repulsion of Impacting Water Droplets", *ACS Nano* (2010), 4(12), pp. 7699-7707.
13. Yoshimitsu, Z., Nakajima, A., Watanabe, T. and Hashimoto, K. "Effects of Surface Structure on the Hydrophobicity and Sliding Behavior of Water Droplets". *Langmuir* (2002), 18, 5818-5822.
14. Johnson, R. E., Dettre, R. H. "In Wetting of Low Energy Surfaces", Marcel Dekker: New York, NY, 1993; pp. 2-71.
15. Wang, S., Liu, K., Yao, X. and Jiang, L. "Bioinspired Surfaces with Superwettability: New Insight on Theory, Design and Applications". *American Chemical Society* (2015), 115, 8230-8293.
16. Malavasi, I., Veronesi, F., Caldarelli, A., Zani, M., Raimondo, M. and Marengo, M. "Is a Knowledge of Surface Topology and Contact Angles Enough to Define the Droplet Impact Outcome?" *Langmuir* (2016), 32, 6255-6262.
17. Shi, Z., Liu, Z. Song, H. and Zhang, X. "Prediction of Contact Angle for Hydrophobic Surface Fabricated with Micro-Machining Based on Minimum Gibbs Free Energy". *Applied Surface Science* (2016), 364, 597-603.

18. Tang, P., Feng, C., Xu, L. and Zhang, J. "Preparation of Hydrophobic Surface on Titanium by Micro-Rolling and Laser Diffusion Carbonitriding". *Applied Surface Science* (2016), Vol. 364, pp. 597-603.
19. Maitra, T., Antonini, C., Tiwari, M. K., Mularczyk, A., Imeri, Z., Schoch, P. and Poulidakos, D. "Supercooled Water Drops Impacting Superhydrophobic Textures". *Langmuir* (2014), 30(36), pp. 10855-10861.
20. Cui, C., Collier, B., Duan, X., Poduska, K., "Hydrophobic Steel Surfaces with Micron-scale and Sub-micron Structures from laser Fabrication", 2nd Thermal and Fluid Engineering Conference, April 2-5, 2017, Las Vegas, NV, USA.
21. Won, G., Song, K., Rahmawan, Y., and Chu, C. "One-Step Process for Superhydrophobic Metallic Surfaces by Wire Electrical Discharge Machining", *ACS Applied Materials & Interfaces*, Vol(4), pp. 3685-3691.
22. Weisensee, P. B., Torrealba, E. J., Raleigh, M., Jacobi, A. M. and King, W. P. "Hydrophobic and Oleophobic Re-entrant Steel Microstructures Fabricated Using Micro Electrical Discharge Machining". *Microeng* (2014), 24, 095020 (10pp).
23. Liu, T. and Kim, C. J. "Turning a Surface Superrepellent Even to Completely Wetting Liquids", *Science* (2014), Vol 346, issue 6213.
24. Varshney, P., Mohapatra, S. S. and Kumar, A. "Superhydrophobic Coatings for Aluminum Surfaces Synthesized by Chemical Etching Process". *International Journal of Smart and Nano Materials* (2016), Vol. 7(4), 248-264.
25. Liu, Y., Yin, X., Zhang, J., Yu, S., Han, Z. and Ren, L. "An Electro-deposition Process for Fabrication of Biomimetic Superhydrophobic Surface and its Corrosion Resistance on Magnesium Alloy". *Electrochimica Acta* (2014), Vol 125, pp 395-403.

26. Worthington, A.M. Proc. R. Soc. London 25 (1876) 261-272.
27. Yarin, A.L. “Droplet Impact Dynamics: Splashing, Spreading, Receding, Bouncing”. Annual Review of Fluid Mechanics (2006). Vol. 38: 159-192.
28. Harlow, F. H.; Shannon, John. “The splash of a liquid drop”. Journal of Applied Physics (1967), 38(10), pp. 3855-3866
29. Trapaga, Gerardo and Szekely, Julian. “Mathematical modelling of the isothermal impingement of liquid droplets in spraying processes”. Metallurgical and Materials Transactions B (1991), 22(6), pp. 901-914.
30. Fukai, J. “Modeling of the deformation of a liquid droplet impinging upon a flat surface”. Physics of Fluids A: Fluid Dynamics (1993), 5(11), pp. 2588-2599.
31. Pasandideh-Fard, M., Qiao, Y. M., Chandra, S., and Mostaghimi, J. “Capillary Effects During Droplet Impact on a Solid Surface”. Physics of fluids (1996), 8(3), pp. 650-659.
32. Shin, S.; Juric, D. “Simulation of Droplet Impact on a Solid Surface Using the Level Contour Reconstruction Method”. Journal of mechanical science and technology (2009), 23(9), pp. 2434-2443.
33. Sidik, N.C. and Rafaty, M.Z. “Numerical Study of Droplet Dynamics on Solid Surface. In: Computer Research and Development”, Second International Conference on. IEEE (2010). pp. 493-496.
34. Guo, Y., Shen, S., and Quan, S. “Numerical Simulation of Dynamics of Droplet Impact on Heated Flat Solid Surface”. International Journal of Low-Carbon Technologies (2012).
35. Wu, H. F., Fichthorn, K. A., and Borhan, A. “An Atomistic–continuum Hybrid Scheme for Numerical Simulation of Droplet Spreading on a Solid Surface”. Heat

- and Mass Transfer (2014), 50(3), pp. 351-361.
36. Jones, H. "Cooling, Freezing and Substrate Impact of Droplets Formed by Rotary Atomization". *Journal of Physics D: Applied Physics* (1971), 4(11), pp. 1657.
 37. Madejski, J. "Solidification of Droplets on a Cold Surface". *International Journal of Heat and Mass Transfer* (1976), 19(9), pp. 1009-1013.
 38. Chandra, S. and Avedisian, C. T. "On the Collision of a Droplet with a Solid Surface". *Proceedings of the Royal Society of London A: Mathematical, Physical and Engineering Sciences*. The Royal Society, 1991. p. 13-41.
 39. Asai, A., M. Shioya, S. Hirasawa, and T. Okazaki, "Impact of an Ink Drop on Paper". *J. Imag. Sci. Tech.*, 37, 205 (1993).
 40. Dupuis, A. and Yeomans, J. M. "Modelling Droplets on Superhydrophobic Surfaces: Equilibrium States and Transitions". 2005.
 41. Karapetsas, G. and Chamakos, N. T. Papathanasiou, "Athanasios G. Efficient Modelling of Droplet Dynamics on Complex Surfaces". *Journal of Physics: Condensed Matter* (2016), 28(8).
 42. Bennett, T. and PoulikAkos, D. "Splat-quench Solidification: Estimating the Maximum Spreading of a Droplet Impacting a Solid Surface". *Journal of Materials Science* (1993), 28(4), pp. 963-970.
 43. Scheller, B. L. and Bousfield, D. W. "Newtonian Drop Impact With a Solid Surface". *AIChE Journal* (1995), 41(6), pp. 1357-1367.
 44. Mao, T., Kuhn, D. C. S. and Tran, H. "Spread and Rebound of Liquid Droplets Upon Impact on Flat Surfaces". *AIChE Journal* (1997), Vol. 43, No. 9.
 45. Sabry, M. and Elgharied, E. "Droplet Dynamics Over a Super Hydrophobic Surface". In: *Thermal Issues in Emerging Technologies Theory and Applications (ThETA)*, 2010 3rd International Conference on. IEEE, 2010. p. 137-143.

46. Bahadur, B., Mishchenko, L., Hatton, B., and Taylor, J. A. "Predictive Model for Ice Formation on Superhydrophobic Surfaces". *Langmuir* 2011, 27, 14143-14150.
47. Alizadeh, A. et al. "Temperature Dependent Droplet Impact Dynamics on Flat and Textured Surfaces". *Applied Physics Letters* (2012), 100(11).
48. Patil, N. D., Bhardwaj, R., and Sharma, A. "Droplet Impact Dynamics on Micropillared Hydrophobic Surfaces". *Experimental Thermal and Fluid Science*, 2016, 74, pp. 195-206.
49. Pravinraj, T., Patrikar, R. "Modelling and Investigation of Partial Wetting Surfaces for Drop Dynamics using Lattice Boltzmann Method". *Applied Surface Science*, 2017.
50. Kulinich, S. A., Farhadi, S., Nose, K. and Du, X. W. "Superhydrophobic Surfaces: Are They Really Ice-Repellent?". *Langmuir* (2011), 27(1), pp. 25-29.
51. Hejazi, V., Sobolev, K. and Nosonovsky, M. "From Superhydrophobicity to Icephobicity: forces and interaction analysis". *Scientific Report 3*, article number: 2194.
52. Nosonovsky, M. and Hejazi, V. "Why Superhydrophobic Surfaces Are Not Always Icephobic". *ACS NANO* (2012), VOL. 6, No. 10, pp. 8488-8491.
53. Hobbs, P. V. "Ice Physics", *Oxford Classic Texts in the Physical Science*.
54. Jung, S., Tiwari, M. K., Doan, N. V. and Poulikakos, D. "Mechanism of Supercooled Droplet Freezing on Surfaces". *Nature Communications*. 3:615.
55. Rioboo, R. T. and Mareng, M. "Outcomes from a Drop Impact on Solid Surfaces". *Atomization and Sprays*, 2001, vol.11, no.2, p155-165.
56. Chen, L. "A Comparative Study of Droplet Impact Dynamics on a Dual-scaled Superhydrophobic Surface and Lotus Leaf". *Applied Surface Science* (2011).
57. Nosonovksy, M. and Bhusan, B. "Energy Transition in Superhydrophobicity: Low

- Adhesion, Easy Flow and Bouncing”. *Journal of Physics: Condensed Matter*, 2008.
58. Hu, J., Xu, K., Wu, Y., Lan, B., Jiang, X., and Shu, L. “The Freezing Process of Continuously Sprayed Water Droplets on the Superhydrophobic Silicone Acrylate Resin Coating Surface”. *Applied Surface Science* (2014), 534-544.
59. Czitrom, V. “One-Factor-at-a-Time versus Designed Experiments”, *The American Statistician*, 53(2), pp. 126-131.
60. Montgomery, D.G. “Design and Analysis of Experiments”, 8th Edition, Wiley.
61. Myers, R. H., Montgomery, D. C., and Cook, C. M. A. “Response Surface Methodology: Process and Product Optimization Using Designed Experiments”, 4th Edition, Wiley.
62. Lye, L. M. “Design of Experiments in Civil Engineering: Are We Still in the 1920’s?”, Annual Conference of the Canadian Society for Civil Engineering, Montréal, Canada.
63. Mokry, S. “Development of a Heat-transfer Correlation for Supercritical Water in Supercritical Water-cooled Reactor Applications”. Proceedings of the 14th international heat transfer conference. August 8-13, 2010, Washington, DC, USA.
64. Li, M., Zhai, J., Liu, H., Song, Y., and Zhu, D. “Electrochemical Deposition of Conductive Superhydrophobic Zinc Oxide Thin Films”. *J. Phys. Chem. B*, 2003, 107(37), pp 9954-9957.
65. Xiang, T., Zhang, M., Li, C., Dong, C., Yang, L., and Chan, W. “CeO₂ Modified SiO₂ Acted as Additive in Electrodeposition of Zn-Ni alloy Coating with Enhanced Corrosion Resistance”, *Journal of Alloys and Compounds*, 2017.

66. Jin, Z., Sui, D., and Yang, Z. “The Impact, Freezing, and Melting Processes of a Water Droplet on an Inclined Cold Surface”, *International Journal of Heat and Mass Transfer* 90 (2015) 439-453.
67. Rioboo, R. T., Marengo, M. and Tropea, C. “Time evolution of liquid drop impact onto solid dry surfaces”. *Experiments in fluids*, 2002.

Appendix I

Detail SolidWorks drawing and BOM of the experimental setup.

ITEM NO.	PART NUMBER	DESCRIPTION	QTY.
1	lift base		1
2	Cold Plate		1
3	Machined Sample		1
4	Thermal Electrical Cooler		1
5	Clamp		1
6	Stand Holder		2
7	Stand		1
8	Temperature Controller		1
9	Thermal Bath		1
10	Syringe Pump		1

APPROVED FOR RELEASE		DATE		DRAWN AND CHECKED BY		CONTROL ENGINEER		REGION	
NAME	DATE	NAME	DATE	NAME	DATE	NAME	DATE	NAME	DATE
SAWAI	10/17/2011	SAWAI	10/17/2011	SAWAI	10/17/2011	SAWAI	10/17/2011	SAWAI	10/17/2011
CHOP		CHOP		CHOP		CHOP		CHOP	
MAR		MAR		MAR		MAR		MAR	
QA		QA		QA		QA		QA	

Icing Experiment Setup

A1